



**CHARACTERIZATION OF FUNCTIONALLY  
GRADED MATERIALS**

THESIS

Benjamin D. Chapman, Second Lieutenant, USAF  
AFIT/GAE/ENY/06-M05

**DEPARTMENT OF THE AIR FORCE  
AIR UNIVERSITY**

***AIR FORCE INSTITUTE OF TECHNOLOGY***

---

**Wright-Patterson Air Force Base, Ohio**

APPROVED FOR PUBLIC RELEASE; DISTRIBUTION UNLIMITED

The views expressed in this thesis are those of the author and do not reflect the official policy or position of the United States Air Force, Department of Defense, or the United States Government.

AFIT/GAE/ENY/06-M05

CHARACTERIZATION OF FUNCTIONALLY GRADED MATERIALS

THESIS

Presented to the Faculty

Department of Aeronautics and Astronautics

Graduate School of Engineering and Management

Air Force Institute of Technology

Air University

Air Education and Training Command

In Partial Fulfillment of the Requirements for the  
Degree of Master of Science in Aeronautical Engineering

Benjamin D. Chapman, BS

Second Lieutenant, USAF

March 2006

APPROVED FOR PUBLIC RELEASE; DISTRIBUTION UNLIMITED

CHARACTERIZATION OF FUNCTIONALLY GRADED MATERIALS

Benjamin D. Chapman, BS

Second Lieutenant, USAF

Approved:

\_\_\_\_\_  
Dr. Anthony Palazotto (Chairman)

\_\_\_\_\_  
Date

\_\_\_\_\_  
Dr. Marina Ruggles-Wrenn (Member)

\_\_\_\_\_  
Date

\_\_\_\_\_  
Dr. Donald Kunz (Member)

\_\_\_\_\_  
Date

### **Abstract**

The purpose of this study was to characterize the behavior of a functionally graded material through experimentation and analytical modeling. Functionally graded materials are a ceramic metal composite which transitions from metal on one face to ceramic on the opposite face. Creating reliable models required verifying the material properties. This was accomplished through the use of a static modulus of elasticity test as well as a dynamic ping test. The natural frequencies from the dynamic test were compared with finite element models to determine which material properties most accurately represented the functionally graded material. It was found that the material properties established experimentally by Hill and Lin produced the best models. A fracture surface was examined to determine the failure criteria for the prediction of failure in a cyclic loading scenario. It was determined that the material would fail in a brittle manner and the maximum principle stresses should be used to predict failure. Finally, a model was generated to analyze the through-the-thickness stresses in the material under a sinusoidal forcing function. It was determined that the majority ceramic upper layer was the critical layer for failure and required an amplitude of 5.83 KN to reach failure in the specimen.

## **Acknowledgements**

I would first like to thank my advisor, Dr. Anthony Palazotto for all of his help and guidance in this endeavor. I would also like to thank my sponsor Dr. Ravinder Chona for his financial support and Dr. Larry Byrd for his help with the experimental set-up and data acquisition. Also my sincere appreciation goes out to Brian Smyers for the microscope photos he provided, to Dr. Richard Cobb for his help setting up the dynamic testing in the vibrations lab, Travis Wyen for his help in the AFRL labs and to Capt Glenn Cooley for his help with the Abaqus software program. Thank you to Lt Col Larry Butkus for his help with examining the scanning electron microscope photographs and to Dr. Steve Russ for his help explaining the effects of adding boron into a titanium matrix. Finally I would like to thank the members of my committee Dr. Marina Ruggles-Wrenn and Dr. Donald Kunz.

Benjamin D. Chapman

## Table of Contents

	Page
Abstract .....	iv
Acknowledgements .....	v
List of Figures .....	viii
List of Tables .....	xi
 I. Introduction .....	 1
Background .....	1
Research Focus .....	5
Research Outline .....	6
 II. Methodology .....	 8
Chapter Overview .....	8
Research Focus and Development .....	8
FGM Theory .....	10
FGM Manufacturing Process and Material Description .....	15
Experimental Setup and Procedures .....	20
Static Experiment Setup .....	20
Dynamic Experiment Setup .....	26
Fracture Surface Examination .....	33
Finite Element Development: Matlab .....	33
Finite Element Development: Abaqus .....	36
Summary .....	46
 III. Analysis and Results .....	 48
Chapter Overview .....	48
Experimental Results .....	48
Static Experiment Results .....	48
Dynamic Test Results .....	54
Damping Results .....	60
Microstructures Results .....	63
Matlab Frequency Results .....	71
Abaqus Frequency Results .....	72
Summary .....	84
 IV. Conclusions and Recommendations .....	 86

	Page
Chapter Overview .....	86
Conclusions.....	86
Recommendations for Action .....	89
Recommendations for Future Research .....	90
Summary .....	91
Appendix A: Matlab Code .....	93
Appendix B: Sample Abaqus Report.....	96
Appendix C: Displayed Node Numbers .....	97
Bibliography .....	98
Vita.....	101

## List of Figures

Figure	Page
1. FGM Orientation.....	2
2. Graphical FGM Representation .....	2
3. Variations in Parameter $n$ .....	12
4. Composition Distribution of Ti-TiB .....	16
5. General Distribution of Whiskers .....	19
6. Whisker Interconnectedness .....	19
7. Cantilevered Beam Setup.....	21
8. Cantilevered Beam with Weights Applied .....	22
9. Cantilevered Beam.....	23
10. Specimen Orientation.....	24
11. Dynamic Cantilever Setup .....	26
12. Cantilever with Spacer.....	27
13. Cantilever without Spacer.....	27
14. Affixed Accelerometer.....	28
15. Signal Conditioner .....	29
16. Signal Processor and PC .....	29
17. SignalCalc Output.....	31
18. Vertical Post Cantilever .....	32
19. Abaqus Beam Element.....	37
20. Mode One Comparison .....	38

Figure	Page
21. Plane Stress/Strain Model .....	39
22. One Thickness Element .....	40
23. Two Thickness Elements .....	40
24. Plate Model .....	41
25. FGM Ply Lay-Up .....	42
26. Maximum Stress Location .....	45
27. Stress Concentrations .....	45
28. Homogeneous Material Modulus of Elasticity Results .....	49
29. Specifications Interpolation Chart .....	50
30. FGM Modulus of Elasticity Results .....	52
31. Sample Matlab Plot (974-1 #1).....	55
32. Damping Coefficient Time History .....	60
33. Magnified Time History Peaks .....	63
34. FGM Side View .....	64
35. Layer Intersection .....	65
36. Fracture Surface .....	67
37. Foil Separation .....	68
38. Upper Fracture Surface .....	69
39. Lower Fracture Surface.....	70
40. Homogeneous Mode 1 .....	76
41. Homogeneous Mode 2 .....	76
42. Homogeneous Mode 3 .....	77

Figure	Page
43. FGM Mode 1.....	77
44. FGM Mode 2.....	77
45. FGM Mode 3.....	77
46. FGM Maximum Stress Location .....	82
47. Forcing Function.....	83
48. Node Numbers .....	97

## List of Tables

Table	Page
1. Layer Thickness and Composition.....	15
2. Ti-TiB FGM Material Properties .....	18
3. Matlab Verification.....	34
4. Abaqus FGM Comparison .....	43
5. Manufacturers Specifications.....	50
6. Dynamic Test Results .....	56
7. Test Specimen Dimensions.....	56
8. Average Dimensions and Natural frequencies.....	58
9. Density Comparison.....	58
10. Clamp Method Comparison.....	59
11. Experimental Damping Coefficient .....	62
12. Matlab Results .....	72
13. Abaqus Specifications Comparison .....	73
14. Model Comparison.....	75
15. FGM Model Comparison.....	78
16. FGM Layer Thickness Variation .....	80
17. Ultimate Strength.....	82

# CHARACTERIZATION OF FUNCTIONALLY GRADED MATERIALS

## I. Introduction

### Background

As technology progresses at an ever increasing rate, the need for advanced capability materials becomes a priority in the engineering of more complex and higher performance systems. This need can be seen in many fields in which engineers are exploring the applications of these new engineered materials. Aerospace engineers trying to incorporate new and improved capabilities into air and space systems are pushing the envelope for what current materials can physically handle. Functionally Graded Materials (FGMs) are a relatively new (circa 1970's) technology and are being studied for the use in components exposed to harsh temperature gradients.

While laminated composite materials provide the design flexibility to achieve desirable stiffness and strength through the choice of lamination scheme, the anisotropic constitution of laminated composite structures often result in stress concentrations near material and geometric discontinuities that can lead to damage in the form of delamination, matrix cracking, and adhesive bond separation. [21]

FGMs alleviate these problems because they consist of a continuous variation of material properties from one surface to the other. The continuous nature of the variation lessens the stress concentrations which become troublesome in a laminated composite material. Also the smooth transition through the various material properties reduces both thermal and residual stresses [20]. In most cases the material progresses from a metal on one surface to a ceramic or mostly ceramic on the opposite surface, with a smooth transition

throughout the center of the material. Also the material properties can change in any orientation across a material, but the majority of applications to date deal with a material in which the properties change through the thickness of the material or in the Z- Axis of material which is depicted in Figure 1 below.

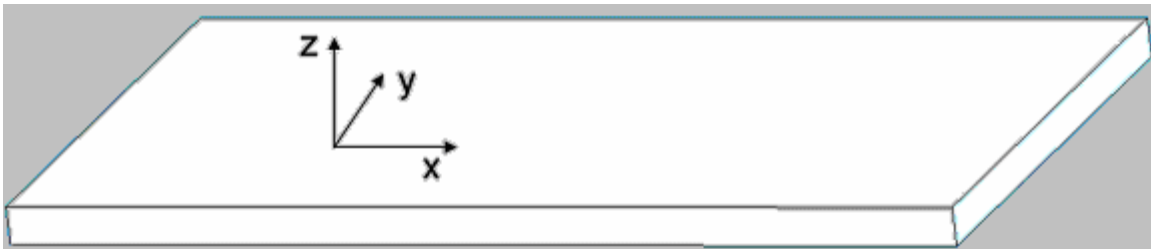


**Figure 1. FGM Orientation**

The material transitions from a metal to a ceramic by increasing the percentage of ceramic material present in the metal until the appropriate percentage is reached or a pure ceramic is achieved (See Figure 2 below).

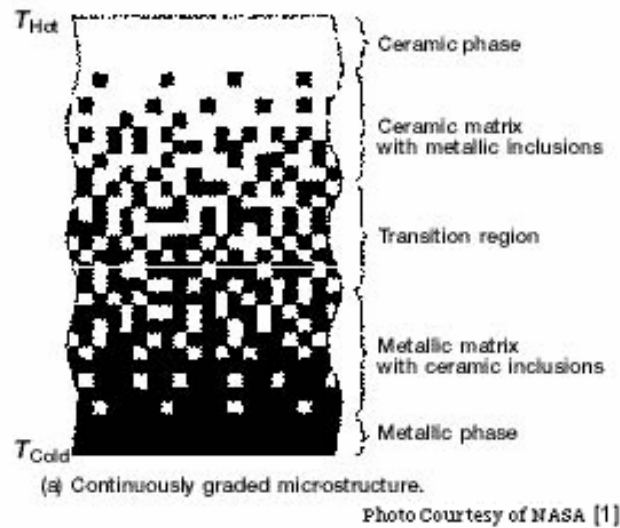


**Figure 2. Graphical FGM Representation**

As seen above, the material does not have a dramatic change in material properties at any one point through the thickness which would cause a large stress

concentration. This material usually exists where there is an extreme temperature gradient which is designated by  $T_{\text{hot}}$  and  $T_{\text{cold}}$  on the figure above. The ceramic face of the material is generally exposed to a high temperature, while the metallic face is usually subjected to a relatively cooler temperature. The smooth transition of material properties allows for a material whose properties provide thermal protection as well as structural integrity without introducing a single point for failure within the structure. This single point of failure is of critical importance in the space program as NASA has used thermal protection tiles laminated to the metallic structure of the space shuttle to handle the extreme temperatures for re-entry into the earth atmosphere. These tiles are susceptible to “cracking and debonding at the superstructure/tile interface due to abrupt transition between thermal expansion coefficients [3].” The smooth transitions between material properties eliminates the potential cracking and debonding of thermal protection tiles laminated to structural members.

The capabilities of the material are quite flexible as one can vary the materials used as well as the function at which they transition from surface to surface. A specific metal and ceramic can be chosen for the particular application to capitalize on the positive characteristics of each of the materials. Also, the function between the two outside materials can be mathematically maximized and tailored specifically to meet the needs of the desired application as seen in the research of Cooley and Palazotto [5].

There are many current and future applications for this material. Some of these include the space shuttle applications as discussed earlier and other aeronautical applications. One of these is the aircraft exhaust wash structures which separate “exhaust gas from aircraft structure for vehicles which have internally exhausted engines, i.e.,

stealth aircraft and UAVs (Unmanned Aerial Vehicles) with engines that don't exhaust directly to the atmosphere [3]." FGMs are being used in the "thermoelectric devices for energy conversion" and the "semiconductor industry [21]." FGMs are also being researched as a possible thermal barrier coating to be used in gas turbine engines [12]. As research into this material progresses and the cost for manufacturing decreases, it is inevitable that many other industries which deal with severe thermal gradients will begin investigating the usefulness of FGMs.

Some of the current research in the FGM field includes the following studies. Reddy [21] worked on characterizing the theoretical formulation of FGMs to include the derivations of equations used to calculate material properties throughout the thickness of the material based on the through the thickness distribution of materials. Na and Kim [16] studied the thermomechanical buckling of FGMs using a finite element discretization method. Eason and Caraballo [7] used finite element analysis to study the thermoelastic behavior of functionally graded structures. Cooley [3] researched FGM shell panels under thermal loading also using the finite element method. Hill and Lin [11] concentrated their research of FGMs in the field of residual stress measurement in a ceramic-metallic graded material using experimental procedures that released residual stresses by making incisions into the material and measuring the resulting change in stress with strain gages. Hill along with Carpenter, Paulino, Munir and Gibeling all participated in studying the fracture testing of layered (as opposed to a continuous function) FGMs [10]. The majority of research into this material has been theoretical involving the finite element method. Little research to date focuses on comparing theoretical results with experimental results as the material manufacturing process has yet

to be optimized. FGMs today are relatively expensive and thus most studies have been limited to a computational analysis for determining the potential behavior of this class of material. Further research is needed to begin to compare the actual behavior of FGMs being produced by industries today with finite element models in order to validate this research.

FGMs have the potential to advance the current capabilities in the area of harsh temperature gradient applications as they exist today. Though, further experimental research is needed to validate or improve the modeling techniques being used today, such as the finite element method.

### **Research Focus**

The research done in this thesis explored the relation between experimental and analytical results when examining FGMs. Most current research deals solely with the analytical or computational solutions to FGM problems. These results although good in theory may not accurately depict the actual behavior in a FGM. Also, today the closest approximation to a true functionally graded material is a material in which the properties and percentage composition of the two materials change in discrete steps (not truly a smooth curve of the function). These steps, although discontinuous, still produce a more gradual change as compared with a ceramic laminated to a metal structure.

Researchers often deal solely with the theoretical FGM which is not completely consistent with what industry is capable of producing at this time. As the process is refined the material will eventually approach a true theoretical FGM. The limitations of today's technology in manufacturing FGMs require that they are examined and tested and

consequently modeled using a realistic, useable method. The focus of this thesis is to compare analytical results, specifically finite element analysis, with experimental testing of FGMs.

## **Research Outline**

Determining the accuracy of the material properties for use in the analytical models required experimentation to be conducted for comparison with the finite element analysis of the material. In order to generate data for comparison with the material specifications and the analytical models, two experiments were conducted. The first experiment was a static experiment to verify the specifications for the modulus of elasticity (a critical material property in determining natural frequency) for each of the specimens. The second experiment involved the dynamic testing of the specimens in order to experimentally determine the first three bending modes of the specimen to compare with the results from the finite element analysis using Abaqus. Also, experimental data was used to determine the damping coefficients of the material.

Research was then conducted to study the affects of the manufacturing process on the layers of the FGM and the material characteristics through the use of a micro-structures analysis. This was completed using a polished specimen to examine the variation of the material layers throughout the thickness. Also, a scanning electron microscope was used to gain insight into the material composition and characteristics of the material by examining the fracture surface of a broken specimen. This study helped determine the mode of failure allowing one to predict failure behavior in the future and to establish which criteria would indicate failure in the Abaqus stress analysis.

In order to determine the validity of the material specifications, finite element models using various material properties were created for comparison with the experimental results. The first step completed in the computational analysis was to perform hand calculations in order to set a baseline and a sanity check for the models being created. Then a Matlab code was generated which was able to handle a beam element with multiple elements. Next, the results from the Matlab code were compared with the Abaqus results for a beam with the same number of elements. The specimen was then modeled in different ways in order to characterize the differences in each method of modeling (i.e. a plate element compared with a two-dimensional plane stress/strain element compared with a beam element). This helped determine the accuracy of the finite element program in modeling FGMs as well as facilitated a way to determine if the material properties provided by the manufacturer were correct. Once adequate material properties were determined, Abaqus was used to examine how stresses due to a sinusoidal forcing function were resisted internally.

## **II. Methodology**

### **Chapter Overview**

The purpose of this chapter is to summarize the studies performed in this research as well as to describe the FGM make-up and the processes used to model and test this material. The theory behind functionally graded materials is explored and some specificities of the FGM examined in this research are discussed. The material properties and manufacturing processes are also included. Finally, the experimental procedures are described as well as the Abaqus studies that were performed to compare with the experimental results helping to characterize the FGM.

### **Research Focus and Development**

Material properties were provided by the manufacturer but required experimental verification. Therefore, a static analysis was completed to experimentally determine the modulus of elasticity for each of the specimens. Once data was collected for all of the specimens, a statistical analysis of the results was completed in order to determine if it was appropriate to make any claims about the material provided in each specimen sheet as compared with what the manufacturer's specifications suggested. It was found that the material properties did in fact vary considerably from those values. Because of this, a dynamic test of the specimens was needed for comparison with results from analytical models created with Abaqus to help determine the material properties.

Both the homogeneous material and the FGM were tested dynamically for comparison with the analytical models. Once the natural frequencies for the first three bending modes were established, it was possible to compare them with the Abaqus results to determine the accuracy of the material properties within the models as well as to determine the best modeling technique for characterizing FGMs. The homogeneous material was tested in order to validate the testing procedures and gain confidence in the results for the FGM.

At this point the material was examined under an optical microscope to identify any material discrepancies that were present. This procedure was useful to verify the thickness of the few individual visible layers to compare with the manufacturer's specifications. Also, one specimen arrived broken from the manufacturer without an explanation as to the breakage (it was shrink wrapped in two separate pieces). Photographs from a scanning electron microscope of the fracture surface were examined to determine the material's failure characteristics, and the potential impact on future dynamic failure tests. It was apparent that through the manufacturing process the titanium lost much of its ductility and in turn the fracture toughness decreased leading to the brittle fracture of a normally ductile material.

In order to create helpful analytical models, it was important to gain confidence in the finite element software program used to generate these models. This included the writing of a finite element software code to fully understand the workings of the finite element method as well as to provide a baseline and tool for verification of the results produced in the more complex Abaqus software program. Once the FEA code had been developed in Matlab, similar models using a beam element were developed in Abaqus.

This comparison gave confidence that the Abaqus models were generating accurate results.

Once the initial beam model was verified, the experimental specimens were modeled in Abaqus. The specimens to be experimentally tested consisted of a homogeneous material which was comprised solely from a material which was 85% titanium-boride (ceramic) and 15% titanium, as well as an FGM which gradually transitioned from pure titanium to the 85% TiB-15% Ti material. The FGM was comprised of seven layers with a varying composition of ceramic and metal throughout the thickness. Results were found for both types of specimen materials within the modeling software. The specimens were modeled in various ways as to determine which method most closely approximated experimental results. Two-dimensional plane stress and plane strain elements were both examined as well as a plate element with a composite make-up. The results from these models were compared with the experimental results to determine the most accurate material property set for the specimens. Once the material properties were verified, a stress analysis was performed using the analytical models to determine the amplitude of a sinusoidal forcing function required to fail the FGM specimens.

### **FGM Theory**

A FGM consists of a material whose properties change from one surface to another according to a smooth or continuous function based on the position throughout the thickness of the material. Most often this material consists of ceramic and metallic constituents. One surface is generally a pure metal while the opposite surface is usually

pure ceramic or a majority ceramic. The metal portion of the material acts in the role of a structural support while the ceramic characteristics provide thermal protection when subjected to harsh temperature gradients. The function describing the material variation throughout the material and more importantly the material property variation makes it possible to tailor the function to suit the needs of various applications.

The continuous change in the microstructure of Functionally Graded Materials (FGMs) distinguish them from the fibre-reinforced laminated composite materials, which have a mismatch of mechanical properties across an interface due to two discrete materials bonded together. As a result the constituents of the fibre-matrix composites are prone to debonding at extremely high thermal loading. Further cracks are likely to initiate at the interface and grow into weaker material selections. [20]

FGMs continuous or nearly continuous gradual change in material properties eliminates these problems, making them a desirable choice for adverse thermal gradient applications.

In order to study FGMs a model must be created that describes the function of composition throughout the material. The *volume fraction*,  $V$ , which describes the volume of ceramic at any *point*,  $z$ , throughout the *thickness*,  $h$ , according to a *parameter*,  $n$ , which controls the shape of the function can be seen in equation 1 below [21].

$$V = \left( \frac{z}{h} + \frac{1}{2} \right)^n \quad (1)$$

It follows that the *volume fraction of metal* in the FGM is  $1-V$ . A graphical representation of various values of the parameter  $n$  can be seen in Figure 3 below.

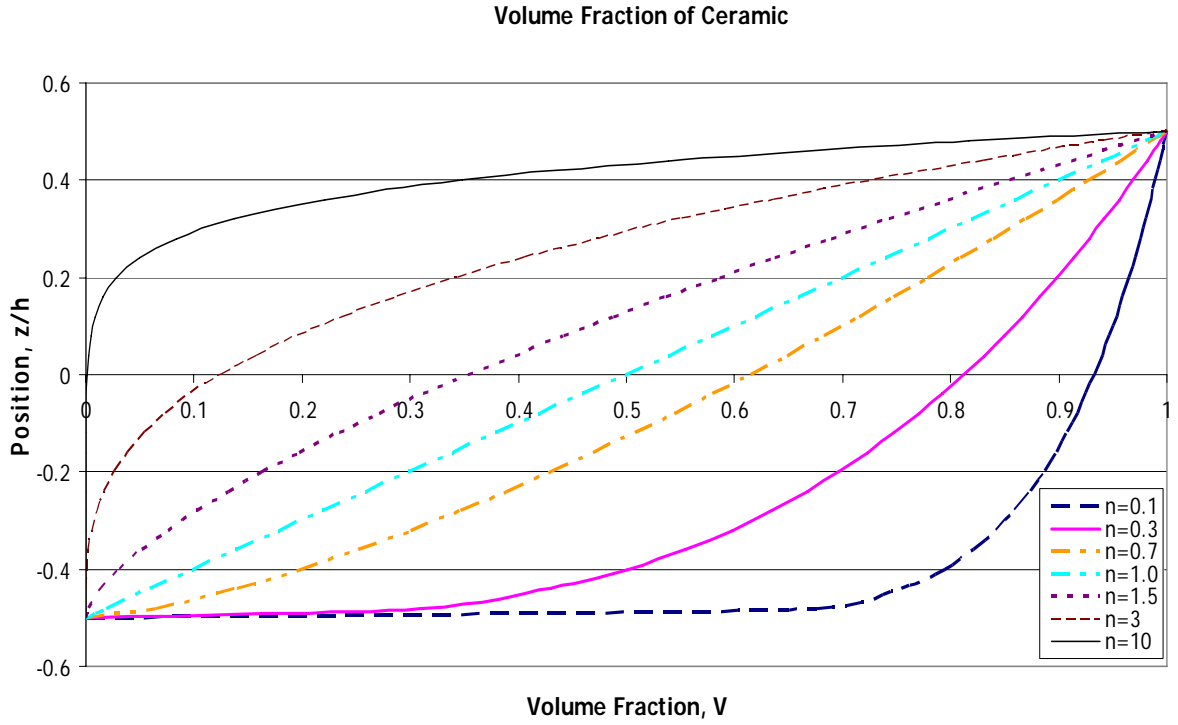


**Figure 3. Variations in Parameter  $n$**

The area to the right of each line represents the amount of metal in the mixture and the area to the left represents the ceramic component of the material. It should be noted that as  $n$  approaches zero the material approaches a homogeneous ceramic, while as  $n$  approaches infinity the material becomes entirely metal. At any point in between zero and infinity the material will contain both metal and ceramic. When  $n$  is set equal to one, the distribution is linear containing equal portions of ceramic and metal. The material properties through the thickness vary as a function of the volume fraction and can be seen in equation 2 below [21].

$$P(z) = (P_t - P_b)V + P_b \quad (2)$$

Where  $P_t$  and  $P_b$  represent the *material property* of the top and bottom respectively.  $P_t$  corresponds to  $P_c$  or the *material property* of the *pure ceramic* and  $P_b$

corresponds to  $P_m$  or the *material property* of the *pure metal*. This equation holds true for the modulus of elasticity, density, thermal expansion, thermal conductivity and Poisson's ratio. Suresh and Mortensen also studied this rule of mixtures approximation and found that a modification improved the accuracy of Young's modulus, "in two-phase composites where one phase is discontinuous in a continuous matrix of the other phase [23]." The Halpin-Tsai equation (3) allows for increased load carrying by the fibers of the matrix and can be seen below [23].

$$E_c = E_2 \left\{ 1 - f_1 \left( \left[ \frac{E_1}{E_2} - 1 \right] \left[ \frac{E_1}{E_2} + \bar{A} \right]^{-1} \right) \right\}^{-1} \left\{ 1 + f_1 \bar{A} \left( \left[ \frac{E_1}{E_2} - 1 \right] \left[ \frac{E_1}{E_2} + \bar{A} \right]^{-1} \right) \right\} \quad (3)$$

Where  $E_c$  is the *composite modulus of elasticity* and  $E_1$  and  $E_2$  refer to each *constituent's modulus of elasticity*. Also,  $f_1$  and  $f_2$  refer to the *volume fraction* of each constituent, "and  $\bar{A}$  is an *empirical parameter* whose magnitude is of the order of unity [23]." These equations become important when determining the material properties for discrete steps in a modeling process as current finite element software cannot handle a true functionally graded structure. The material property for the center of the discrete layer within the beam should be determined using the above approaches and applied to the entire layer of the FGM.

A few other important parameters can be determined using the  $n$  value. One parameter is the total composition of the material as a percentage of ceramic. This helps the engineer gain an understanding of the basic characteristics of the material. This equation (4) can be seen below [5].

$$V_{total, ceramic} = \frac{1}{n + 1} \quad (4)$$

Another valuable parameter which can be determined from the value of  $n$  is the average material property throughout the thickness. This is found by substituting  $V_{total,ceramic}$  for  $V$  in equation 2 above. This can be used for quick calculations treating the material as homogeneous such as solving for the weight of a functionally graded structure. The density (or any other material property) can be determined using equation 5 below [5].

$$P_{average} = \frac{P_t - P_b}{n + 1} + P_b \quad (5)$$

Another quantity that an engineer might be interested in for modeling or judging the basic properties of the material is the point within the FGM at which the volume fraction transitions from mostly metal to mostly ceramic. This equation (6) can be seen below [5].

$$\frac{Z_{transition}}{h} = 0.5^{1/n} - \frac{1}{2} \quad (6)$$

An engineer can use any of these values as a goal or a projected need for the material and solve for the value of  $n$  which satisfies that need in the particular application. The  $n$  value along with the materials used defines the characteristics of the material and can be tailored to produce desired results. “Structural designers requiring significant thermal protection should consider low values of  $n$  which will yield a ceramic rich panel [5].” Conversely the opposite holds true for the designer who wishes to produce a structurally sound material with slightly less thermal protection.

## FGM Manufacturing Process and Material Description

The manufacturing process for FGMs is still in the experimental stages as the material is relatively new and industry has not converged to a single effective solution. Some of the techniques being used today include: “chemical vapor deposition, powdered metal sintering, high-temperature plasma spraying, self-propagating combustion synthesis (SHS), thermo-chemical diffusion, and sedimentation of slurried powders [10].” Despite the many methods to produce a true FGM, “synthesis of materials with a continuous variation in the relative volume fractions of the two constituents may be difficult [10].” Due to the difficulty of producing a truly smooth FGM function throughout the structure, the material used in this thesis consisted of a discrete layered function made of titanium and titanium-boride (Ti-TiB).

The Ti-TiB FGM had one face of pure titanium and the opposite face composed of 15% titanium and 85% titanium-boride. The specimens were each approximately 3.175 mm thick and were composed of seven discrete layers throughout the thickness. The dimensions of the individual layers and percent composition of TiB can be seen in Table 1 below.

**Table 1. Layer Thickness and Composition**

Layer Number	% TiB	Thickness (mm)
1	85	0.9398
2	75	0.4064
3	60	0.4064
4	45	0.4064
5	30	0.4064
6	15	0.4064
7	0	0.2032

It should be noted that the top layer is over twice as thick as the inner layers and the bottom layer (commercially pure titanium) is half the thickness of the inner layers.

The composition distribution is nearly linear as can be seen by the trend-line overlying the actual discrete steps of the material in Figure 4 below.

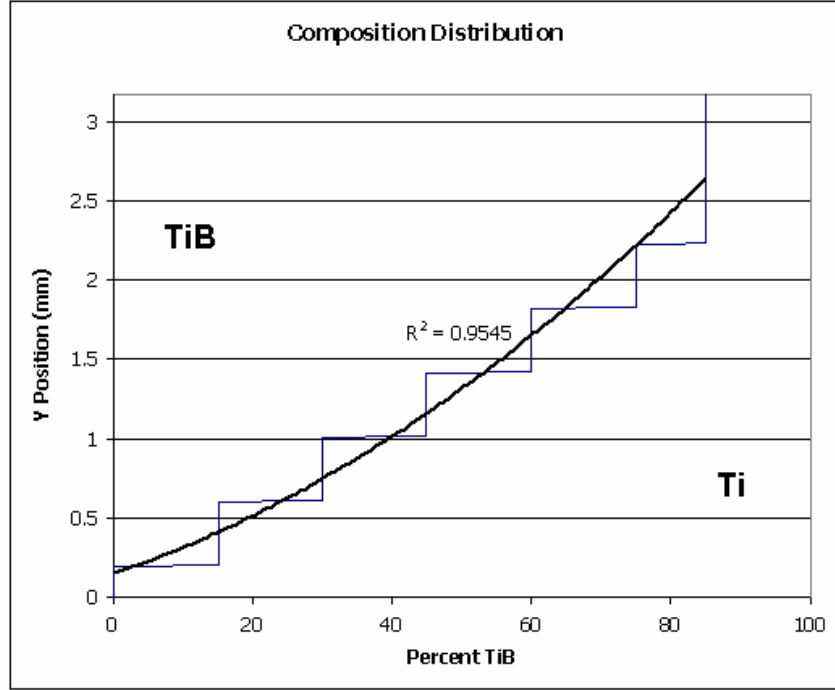


**Figure 4. Composition Distribution of Ti-TiB**

The area to the right of the curve represents the amount of Ti present at that position throughout the thickness, and the area to the left of the curve represents the amount of TiB present in the material at that point. The trend line is a second order polynomial which fits the curve with an  $R^2$  value of 0.9545. The  $R^2$  value is a *predictor value* that ranges between zero and one with one being a perfect prediction for the model. This value is expressed by equation 7 below [22].

$$R^2 = 1 - \frac{SS_{error}}{SS_{total}} \quad (7)$$

Where  $SS_{error}$  is the *variability* about the *predicted values* from the trend-line and  $SS_{total}$  is the *variability* about the *mean*. A value of 0.9545 means the second order

polynomial closely approximates the curve and that about 95% of the variation can be predicted with the trend-line, but because of the stepped nature of the true function it is difficult to fit a smooth trend-line with greater precision. It can be seen that this material does not have a function that coincides directly with theoretical models, or a specific  $n$  value. Although it should be noted that when compared with Figure 3 above, the  $n$  value was estimated to be between 0.7 and 1.0 implying that this FGM tends towards a slight ceramic majority. The approximate  $n$  value for this material is useful in comparing with other FGMs, but because of the discrete nature of the layers and the known composition of each layer, the  $n$  value is not needed for the estimation of material properties and percent compositions at each position throughout the material. Material properties for each of the layers were found by Hill and Lin using an experiment using the identical material produced by the same manufacturer (Cercom, Inc). The material properties which include the:

Elastic modulus and Poisson's ratio were determined for each layer by slicing thin beams from the FGM. Specifically, bilayer beams were made from Layers 1 and 2 and from Layers 6 and 7. Trilayer beams were cut from Layers 3, 4 and 5. Longitudinal and transverse strain gages were bonded to the beams which were then loaded in four point bending. Composite beam theory was used with the resulting strain data to determine elastic modulus and Poisson's ratio for each layer. [11]

This information can be seen in Table 2 below. The slicing method used by Hill and Lin could have effected the results slightly. Though, the amount is unknown and the results they arrived at closely modeled the actual FGM in Abaqus. Therefore it was determined that although the process they used may not have been ideal, they were able to achieve relatively accurate material properties.

**Table 2. Ti-TiB FGM Material Properties**

Layer	% Ti	% TiB	E (GPa)	$\nu$	$\rho$ (kg/m <sup>3</sup> )
1	15	85	274.3	0.170	4561.5
2	25	75	247.6	0.182	4562.5
3	40	60	193.7	0.216	4564.0
4	55	45	162.2	0.246	4565.5
5	70	30	139.4	0.276	4567.0
6	85	15	120.1	0.310	4568.5
7	100	0	106.9	0.340	4570.0

The densities in the table above were interpolated from data found by Chandran, Panda and Sahay in their research with TiB [2]. This material was prepared by Cercom, Inc. which is now BAE Systems Advanced Ceramics located in Vista, CA.

Tape cast layers composed of various mixtures of Ti and titanium-diboride (TiB<sub>2</sub>) powders were placed on top of this plate and the assembled laminate was hot pressed at 1578 K at a pressure of 13.8 MPa. In order to facilitate densification at this temperature, a proprietary sintering aid containing nickel was added to the starting powders. This material created a liquid phase at 1215 K that also catalyzed the reaction of Ti and TiB<sub>2</sub> to form TiB with virtually no residual TiB<sub>2</sub>. [11]

All of the material containing TiB was machined flat and then a 0.2032 mm titanium foil was attached [17].

The use of TiB as a reinforcement is attractive because there is no intermediate phase between titanium and TiB and the formation of TiB requires far lower amount of boron compared to TiB<sub>2</sub>. Further, the relatively lower temperatures involved in solid-state composite processing (900-1,100°C) offer manufacturing ease. In addition, TiB forms as long, pristine single-crystal whiskers in the titanium matrix. This means that, on the basis of the theories of stiffening and strengthening by whisker reinforcement, large increases in composite modulus and strength can be obtained with a relatively smaller amount of reinforcement. [2]

These whiskers can be seen in Figure 5 below. Also it can be seen in Figure 6 that the whiskers can interconnect if the volume ratio of TiB is high enough in the titanium matrix.

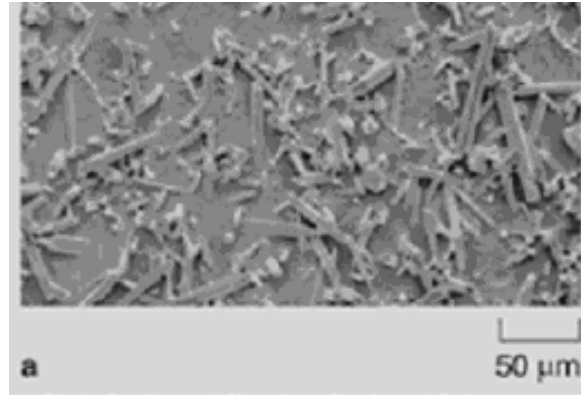


Photo Courtesy of Chandran, Panda and Sahay [2]

**Figure 5. General Distribution of Whiskers**



Photo Courtesy of Chandran, Panda and Sahay [2]

**Figure 6. Whisker Interconnectedness**

This Ti-TiB material closely approximates a true FGM while using small discrete steps to ease in the manufacturing process. Also the thermal expansion properties are relatively similar (Ti CTE is  $8.2 \times 10^{-6}/^{\circ}\text{C}$  and the TiB CTE is  $6.2 \times 10^{-6}/^{\circ}\text{C}$ ) which means there is less of a stress concentration at the intersection of the two materials under high thermal loads. Another important feature is that the crystallographic relationship between titanium and titanium boride makes the interface between the materials clean [19].

Specimens of the same dimensions as those above with a homogenous composition of 85% TiB and 15% Ti were also provided by the manufacturer and were

used in the experiments of this thesis. These specimens were produced the same way as the individual layers are produced in the FGM but without combining the layers and using only the outermost majority ceramic composition.

### **Experimental Setup and Procedures**

Two experiments were required in order to acquire data sufficient to validate the FGM analysis completed in Abaqus. The first experiment consisted of a simple setup used to determine the actual modulus of elasticity of each of the specimens. The manufacturer provided a list of material properties but this experiment was required to verify those values as the FGM manufacturing process is extremely new and the Abaqus software is sensitive to small changes in the modulus of elasticity.

#### ***Static Experiment Setup.***

The first experiment consisted of a cantilevered beam set up as seen in Figure 7 below.

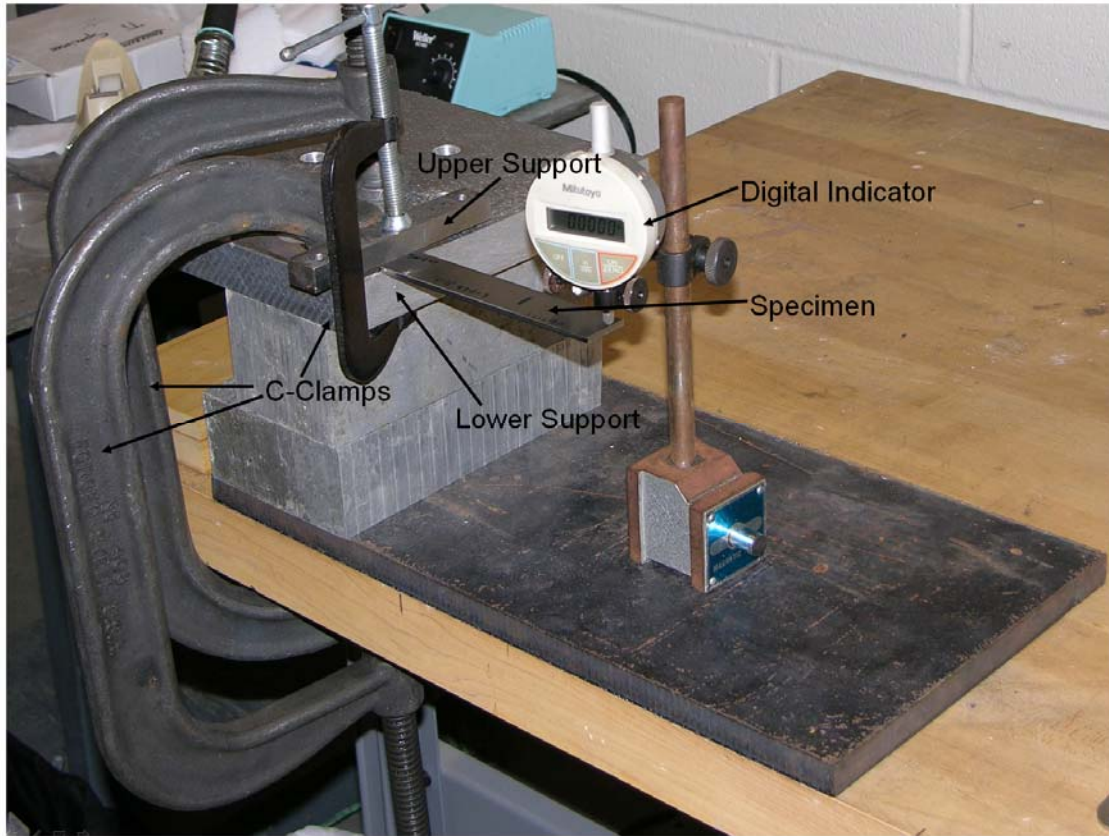


**Figure 7. Cantilevered Beam Setup**

The setup included three aluminum blocks used as spacers. A steel plate used as an anchor for the magnetic base of a Mitutoyo digital indicator. Two large C-clamps used to fix all of the blocks together to insure no slippage of the assembly. One small steel block used as the upper support for the cantilever and an aluminum spacer. The spacer surrounded the specimen in-between the upper and lower contacts of the cantilever and insured that the cantilevered beam was inserted into the same place every time. A small C-clamp was used to secure the upper support of the cantilever. The specimen was then inserted into the clamp and tightened by hand. Because of the imperfect clamping method (ductility of metal supports, C-clamp hand tightened, etc) the results obtained by this experiment were slightly lower than expected. The digital indicator was then placed

at the tip of the beam to measure the deflection at the tip of the beam. Weights were then affixed to the end of the beam using a string and a sharpened paper clip to insure the weight was applied at the specific point of interest. Because the weights were able to swing freely about the tip of the paper clip, the center of gravity, based on the laws of physics, came to rest directly below the tip of the paper clip. This created a vertical downward point force with no moment or horizontal force applied to the end of the beam (Figure 8).



**Figure 8. Cantilevered Beam with Weights Applied**

This setup was first tested with a beam made of 2024 aluminum with known material properties to insure that the setup would produce accurate results. The aluminum beam had dimensions of 10.08cm x 1.27cm x 0.15 cm and deflected 0.4mm

with an applied load of 50 grams. These measurements produced an experimental value of 73.7 GPa for the modulus of elasticity when the theoretical value was 73.1 GPa [13]. This was only a 0.77% difference which suggested that the experimental setup was able to produce accurate results. The method used to solve for the modulus of elasticity from the deflections in the experiment made use of the following equation [8].

$$E = \frac{Wl^2}{6yI}(2l + 3b) \quad (8)$$

The variables are defined by Figure 9 below.  $W$  is the *force applied* (in Newton's) while the other dimensions are all in meters. This same equation holds true for the more specific case where the force is applied at the tip of the beam in which case  $b$  was equal to zero and  $l$  was the *length* of the beam.

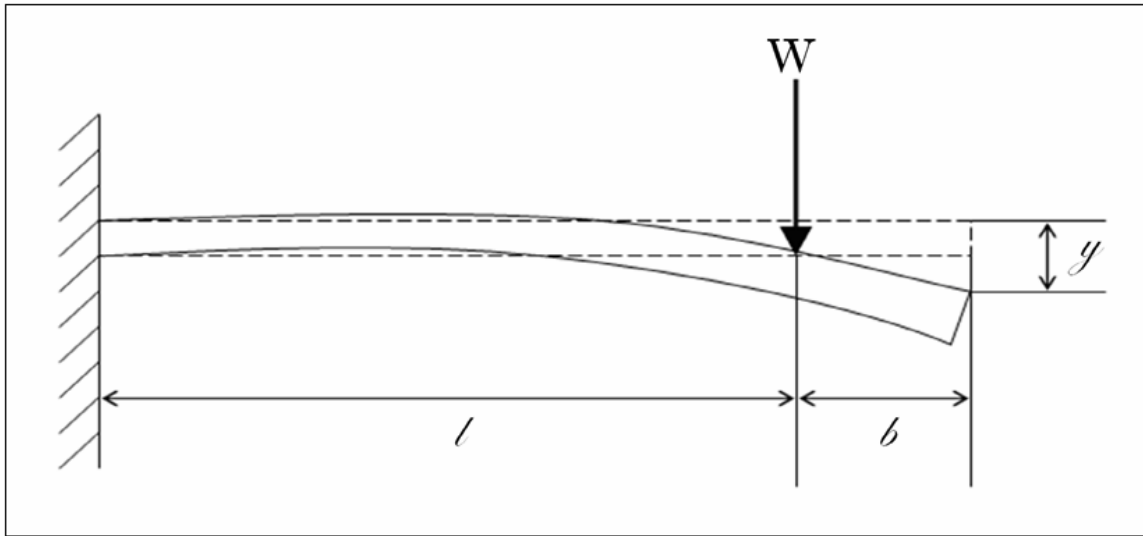


**Figure 9. Cantilevered Beam**

Once the setup was verified the actual specimens were each individually tested. The specimens consisted of two sets of Ti-TiB (homogeneous material consisting of 85% TiB and 15% Ti) which each had seven specimens. Six of which were approximately

12.7cm x 2.54cm x 0.3175cm and one which was 15.24cm x 2.54cm x 0.3175cm all cut from the same sheet of material as seen in Figure 10 below. The cutting of the specimens actually changed the above stated dimensions slightly as those would be the dimensions if the blade used to cut the specimens had zero width. This was accounted for in the analysis section of this thesis. Also, the blade chipped some of the edges of the specimens creating geometries which were not symmetric and which were assumed to have an impact on the testing of the specimen. The chipping of the edges reduced the cross-section and subsequently lowered the effective second moment of inertia which lowered the values for the natural frequencies of the beams in the dynamic tests as was expected.

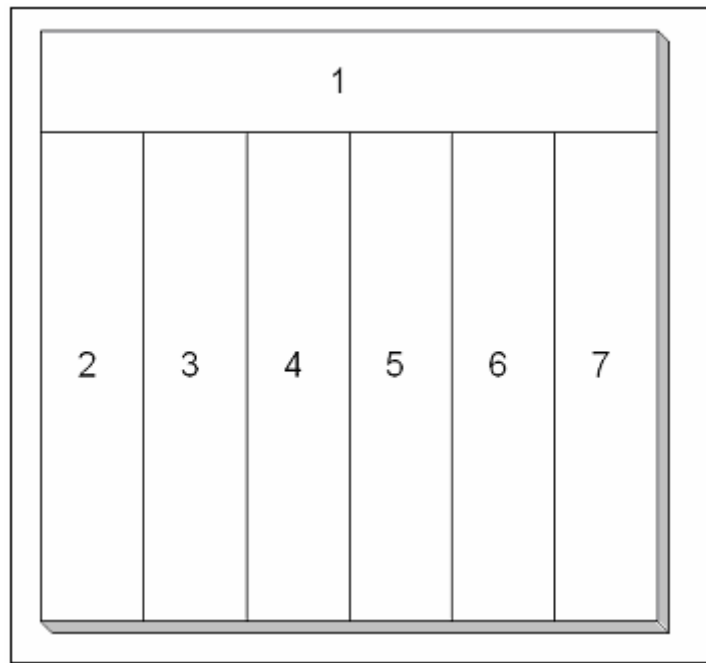


**Figure 10. Specimen Orientation**

Two sets of the FGM specimens were also tested. The orientation for the specimens was the same, but one set was delivered from the manufacturer with a broken

specimen (number seven), so only six specimens from that set were able to be tested. Each specimen was measured with calipers individually to acquire each exact dimension as each specimen varied slightly due to the manufacturing process. Each specimen was also measured once in the apparatus in order to insure the measurements from the digital indicator were taken at the same distance from the cantilever support. Data was recorded for each specimen with two different weights attached to the end of the beam to give different displacements for the analysis. Both weights were applied to the beam twice to insure the readings from the digital indicator were correct. One flaw in the setup was the lack of resolution in the digital indicator. The indicator was only capable of giving readings down to 0.0127 mm which created some problems in the accuracy of the readings but it was determined that the resolution would suffice for the intended purpose of the experiment. Please see the data and analysis for all of the specimens in the Analysis and Results section of this thesis.

Another static experiment was conducted in order to verify that the densities found by Chandran, Panda and Sahay were correct. This simple experiment consisted of weighing each of the specimens on an Ohaus digital scale and then dividing the mass, in kilograms, by the volume. The volume was calculated for each specimen by using the individual dimensions found with the calipers.

### ***Dynamic Experiment Setup.***

The second experiment was a dynamic experiment used to verify the material properties and to determine how well Abaqus could model an actual FGM in a dynamic analysis. The experiment consisted of the cantilevered support seen below (Figure 11).

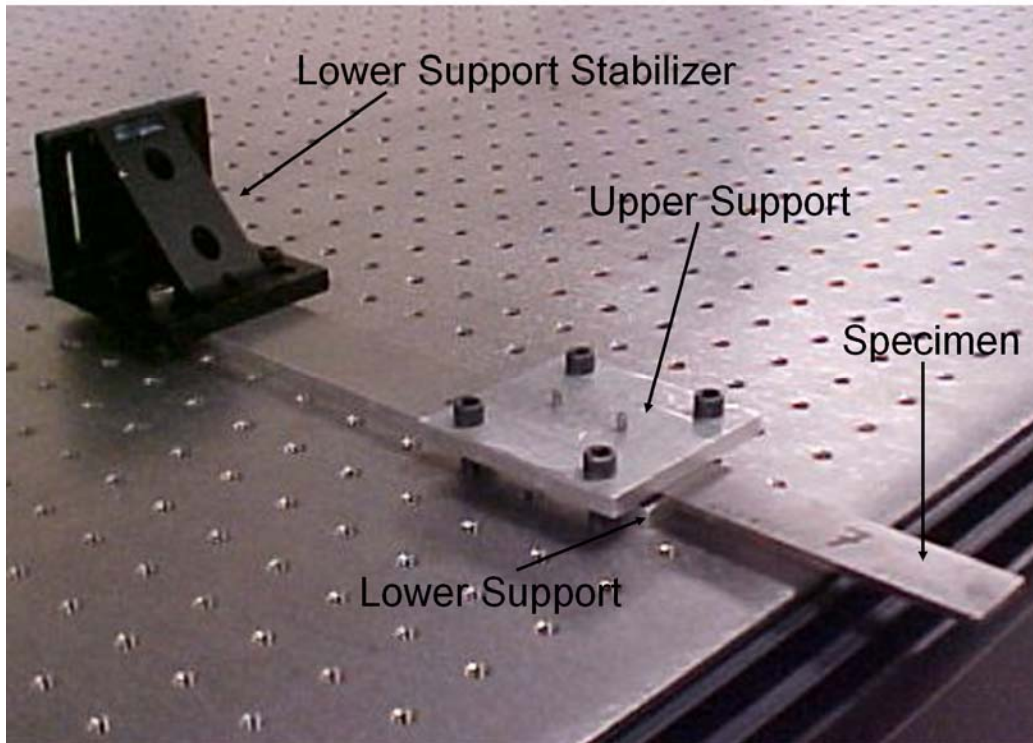


**Figure 11. Dynamic Cantilever Setup**

The setup consisted of a 0.635cm aluminum block bolted to an optical table to create the lower support of the cantilever. A stabilizer was bolted to the far end of the lower support to steady the support and to insure that it did not move when the upper support was loosened for removal of the specimen. Another aluminum block was bolted with its end flush with the bottom support to create the upper support of the cantilever. One of the broken pieces of the specimen from the manufacturer was placed between the bolts at the back of the clamp and was used as a spacer. The specimen was then placed

into the clamp such that exactly 10.16cm protruded from the clamp in the case of the 12.7cm specimens (12.7cm protruded in the 15.24cm specimens). The spacer insured that the clamp created as close to a cantilevered support as possible (Figure 12). Without the spacer, the clamp did not secure the specimen at the tip of the clamp, creating a condition that was difficult to model in the finite element software program (Figure 13).

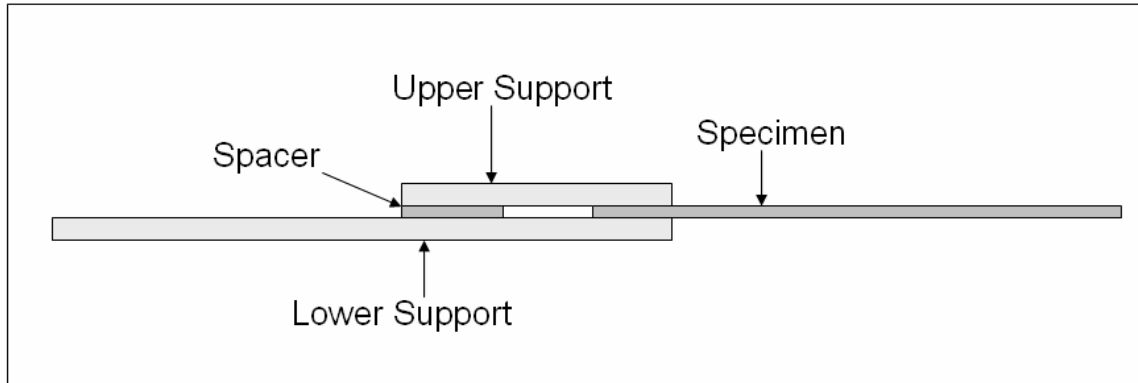


**Figure 12. Cantilever with Spacer**

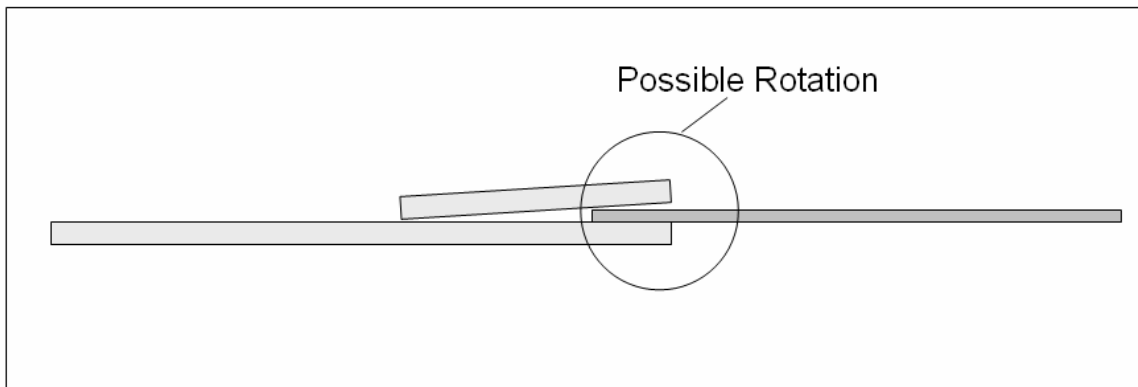


**Figure 13. Cantilever without Spacer**

Once the specimen was securely fastened into the clamp and the bolts were tightened by hand to insure no slippage occurred during the experiment, an accelerometer was attached to the beam as seen in Figure 14 below.

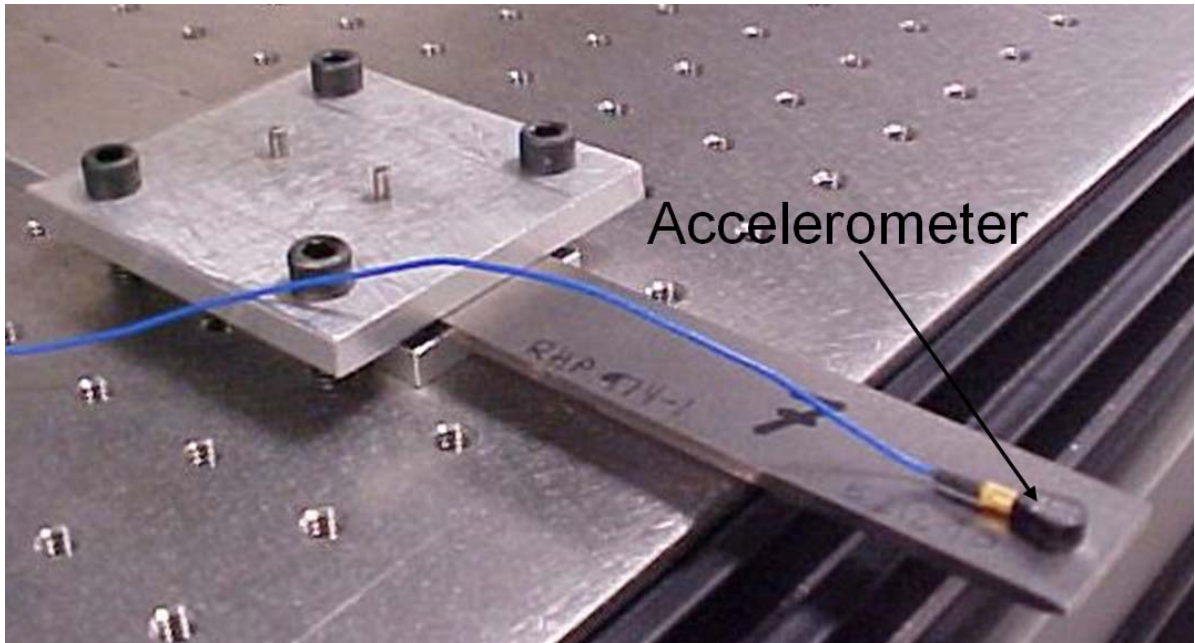


**Figure 14. Affixed Accelerometer**

Bees wax was used to attach the accelerometer to the beam near the tip. Bees wax allowed the ability to quickly apply and detach the accelerometer with virtually no interference with the beam frequencies. The accelerometer was a PCB Piezotronics Inc model 353C22 shear accelerometer with conversion factor of 9.67 mV/g. The conversion factor allowed the determination of the number of g's as a function of millivolts (mV), and subsequently the acceleration the beam was experiencing at the accelerometer. The accelerometer was plugged into a PCB Model 482A16 signal conditioner (Figure 15).



**Figure 15. Signal Conditioner**

Once the signal passed through the conditioner it entered the Hewlett Packard E8408A VXI Mainframe signal processor which took samples of the data and then used SignalCalc 620 software to create plots using the acceleration data in the form of voltages from the accelerometer (Figure 16).

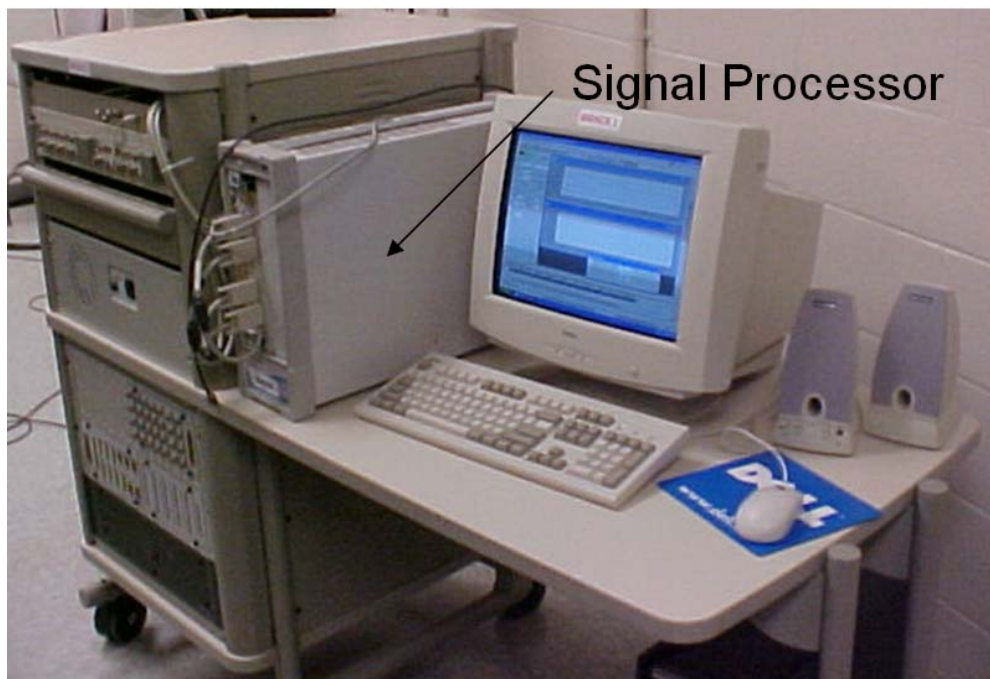


**Figure 16. Signal Processor and PC**

Once the accelerometer was attached and all the equipment was turned on, the program was started. The program was set to take 800 data points over a span of 8000 Hz to insure the inclusion of the first three bending modes. Data was recorded by the software over a span of one tenth of a second during this test run. Because of the broader range of data values (0-8000 Hz) and the limitations of the software, only approximate frequencies were found. Values for frequencies were recorded every 10 Hz which gives an inadequate approximation for the first two modes. Therefore a higher resolution test was required in order to achieve more precise results for the first two natural frequencies. This run included taking 3200 data points over a span of 4000 Hz which increased the resolution to four data points for every five Hertz. Data was recorded for a span of eight tenths of a second and produced results for the lower two modes. An approximation to 10 Hz, from the first test run, produced sufficient data for the third mode and did not require a higher resolution test. The third mode occurred at over 6000 Hz and an interval of 10 Hz is able to produce results with an error band of less than 0.2% of the true frequency. This was deemed sufficient to compare with the Abaqus models.

The software program was programmed to wait in an idle mode for an initial input from the accelerometer to begin taking data (i.e. the program did not record data until there was a signal to record). An Allen Wrench was then used to tap the beam in order to excite vibrations within the beam and, in turn, the accelerometer. As the beam began to vibrate, the program recorded a time history of the accelerations in the form of a voltage output from the accelerometer. From this raw time domain data, a fast Fourier transform was performed by the SignalCalc software program and transformed the data into the frequency domain. From this data it was possible to identify the natural frequencies by

plotting the frequency data and then selecting the frequencies at which the large peaks occurred, as seen in the sample output of Figure 17 below.

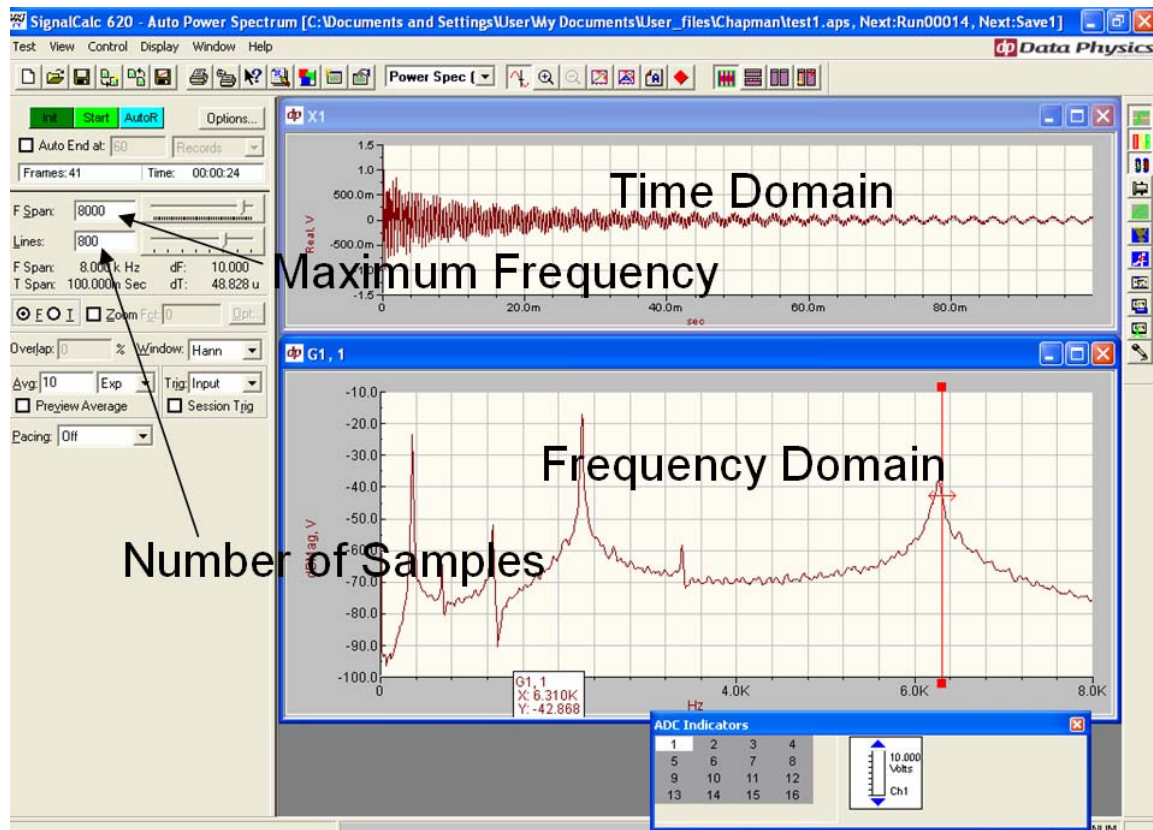


**Figure 17. SignalCalc Output**

The frequency data was averaged over a span of ten test runs, while the time domain data was the result of the last test run completed for the specimen. The output for each run was saved as a .MAT file for analysis in Matlab. Three specimens were tested from each sheet of material (two sheets of FGM and two sheets of homogeneous 85% titanium-boride). The three different specimens from each sheet were chosen to be tested in order to analyze whether or not the position within the sheet or the orientation of the specimen affected the natural frequencies. It was possible that the inner portions of the sheet produced different results than the outer portions due to the manufacturing process.

The edges tend to cool more rapidly than the center of the material and can produce slightly different material properties. Also, the orientation within the sheet could have made an impact on the material properties due to the manufacturing process. Because of this, the horizontal specimen (number one) as seen in Figure 10 was tested to examine the effects of orientation on the natural frequency and a middle specimen as well as an edge specimen (four and seven for the homogeneous specimens, four and two for the FGM) were tested to determine if position within the sheet of material effected the natural frequencies.

One test was then completed that used a different method of clamping. The test was completed the same way as above except the beam was cantilevered on a vertical post with a magnetic base (Figure 18).

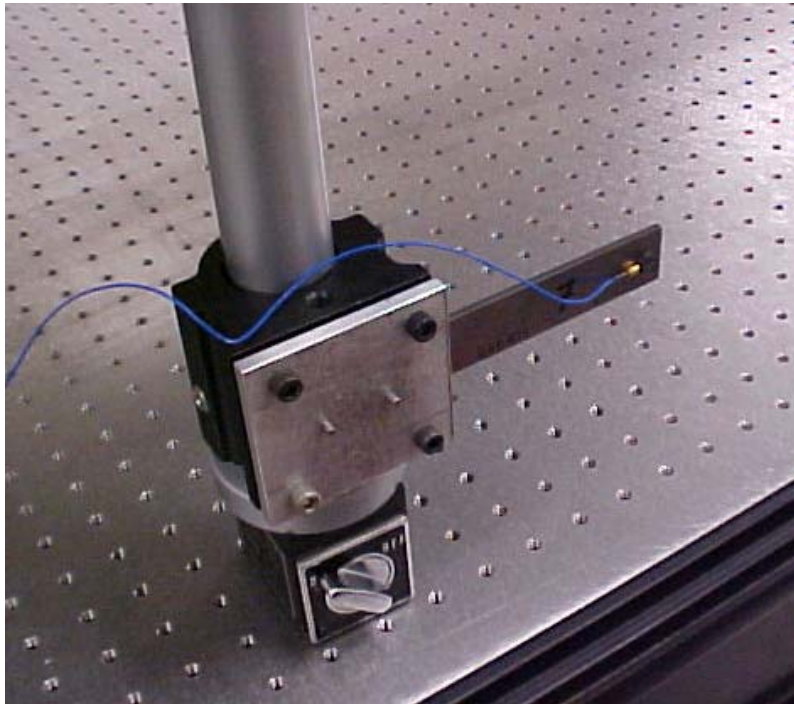


**Figure 18. Vertical Post Cantilever**

This experiment was completed using one set of specimens from the same sheet of material tested in the above manner in order to determine the effects of the clamp on the results of the test.

#### ***Fracture Surface Examination.***

One of the FGM specimens was shipped from the manufacturer broken which provided an opportunity to study the material gradation under an optical microscope. Also the fracture surface was examined under a scanning electron microscope (SEM) to determine the cause of the failure and to examine the failure characteristics of the material. This was completed to make predictions for the expected failure mode for future testing of this FGM. One of the non-fractured edges was sanded and polished in order to view the material free from the residual marks of the manufacturing process (rough edges and grooves from a cutting device, etc). Photographs were taken through a microscope at 50 and 200 times magnification. The fracture surface was cleaned and examined, as shipped, under a SEM in order to see the characteristics of the fracture to determine the interesting features of the fracture surface and predict the effect this could have in the future testing of this material.

#### **Finite Element Development: Matlab**

A simple finite element analysis code was created in Matlab in order to gain confidence in the results generated from the Abaqus models. This code allowed the investigation into the exact workings in finite element analysis. Though the program was not written to handle complex geometries or meshes it was versatile enough to handle any beam geometry with varying numbers of elements. A beam with a single element was

initially compared with a hand calculation to verify the results produced from the Matlab code were accurate (see equation 9 [6]).

$$\omega_1 = 3.533 \left( \frac{EI}{mL^3} \right)^{1/2} \quad (9)$$

The natural frequency produced by this was then divided by two  $\pi$  in order to convert the units from radians per second to Hertz. This allowed a comparison to the Matlab results. The dimensions used in the verification run for both the hand calculations and the Matlab code were 10.16cm x 2.54cm x 3.175cm with a modulus of elasticity of 120 GPa and density of 4430 kg/m<sup>3</sup> (Ti-6Al-4V titanium alloy [9]). The results from verification can be seen in Table 3 below.

**Table 3. Matlab Verification**

	<b>Natural Frequency (Hz)</b>
Hand Calculations	259.849
Matlab FEA Program	259.829
<i>Percent Difference</i>	<i>0.0077</i>

The percent difference seen above shows that the Matlab FEA program produced excellent results when one beam element is used.

The Matlab code required the dimensions of the beam, the appropriate material properties, and the number of elements desired for the analysis. The program could handle any number of elements, but in order to speed up the processing time and decrease the size of the matrices it was best to use 50 or fewer elements. The code then created a connectivity matrix which defined which nodes were connected. Each element had two nodes and every node had identical behavior as the node in which it was connected. The

code then created an individual stiffness matrix for each element and assembled a global stiffness matrix using the individual stiffness matrix seen in equation 10 below [6].

$$[k] = \frac{EI_z}{L^3} \begin{bmatrix} 12 & 6L & -12 & 6L \\ 6L & 4L^2 & -6L & 2L^2 \\ -12 & -6L & 12 & -6L \\ 6L & 2L^2 & -6L & 4L^2 \end{bmatrix} \quad (10)$$

Individual mass matrices were also created for each element and then assembled into a global mass matrix using the consistent mass matrix seen below [6].

$$[m] = \frac{m}{420} \begin{bmatrix} 156 & 22L & 54 & -13L \\ 22L & 4L^2 & 13L & 156 \\ 54 & 13L & 156 & -22L \\ -13L & -3L^2 & -22L & 4L^2 \end{bmatrix} \quad (11)$$

The Choleski Method was then used to manipulate the global mass matrix into a form such that  $[M] = [U]^T[U]$ , where  $[U]$  was an *upper triangular matrix*. The algorithm used to create the  $[U]$  matrix is seen below [6].

$$U_{11} = \sqrt{A_{11}} \quad (12)$$

$$U_{1j} = A_{1j} / U_{11} \quad \text{for } j = 2, 3, \dots, n \quad (13)$$

$$U_{ii} = \left( A_{ii} - \sum_{k=1}^{i-1} U_{ki}^2 \right)^{1/2} \quad \text{for } i = 2, 3, \dots, n \quad (14)$$

$$U_{ij} = \frac{1}{U_{ii}} \left( A_{ij} - \sum_{k=1}^{i-1} U_{ki} U_{kj} \right) \quad \text{for } j = i+1, \dots, n \quad (15)$$

The matrix  $[U]$  was required to manipulate the global mass and stiffness matrices such that  $[K]$  was in essence divided by  $[M]$ . The matrix math slightly complicated the process and required pre and post multiplications of the inverse of the  $[U]$  matrix which

was simply a transformation of the  $[M]$  matrix in order to create a matrix whose eigenvalues were the square of the natural frequencies (see following equation [6]).

$$[K_u] = [U]^{-T} [K] [U]^{-1} \quad (16)$$

Once the matrix  $[K_u]$  was created, the Matlab program solved for the eigenvalues and then calculated the natural frequency, in Hertz, by taking the square root and dividing by two  $\pi$ . The code for this process can be seen in Appendix A.

This program was useful for confirming results from the Abaqus software program's beam element, as it can be easy to miss small details and nuances within the program or incorrectly input information into Abaqus producing inaccurate results. This code also functioned as a sanity check for the results produced in the more complicated plate analysis and 2-D plane stress/strain analysis within the Abaqus software.

### **Finite Element Development: Abaqus**

The Abaqus finite element development began with a simple beam element to compare with the Matlab analysis to insure the correct natural frequencies could be developed in this complex and versatile software program. The beam element, which can be seen in Figure 19 below, was comprised of a homogeneous material allowing for the comparison with the Matlab software program. The beam element is an element that allows for the variation of length, width and height. The beam element "is a long, slender structural member generally subjected to transverse loading that produces significant bending effects as opposed to twisting or axial effects [13]." Each element had four degrees of freedom including two vertical and two rotational at each node. The left end

of the beam was cantilevered, so all degrees of freedom were restricted at that end. The right end of the beam was unrestricted and allowed for both the vertical movement and the rotation of the tip.

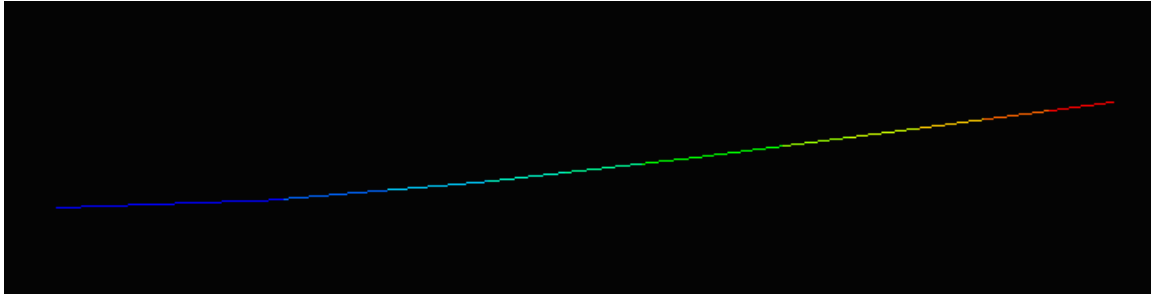


**Figure 19. Abaqus Beam Element**

The material used in this model was a homogenous 85% TiB 15% Ti material with the dimensions of 10.16cm x 2.54cm x 0.3175cm and material properties as defined in Table 2 above. Also the value for the shear modulus was required for the simulation in Abaqus. A value of 20 GPa was used for the shear modulus and was obtained through an interpolation from the manufacturers specifications as the specific shear modulus was not supplied for each individual layer [18]. This value needed only to be approximate for comparison with the Matlab results. Once this beam element was created a study was completed to determine the convergence of the mesh size for both the Abaqus and Matlab models. Values for the first mode with a various number of elements were examined in both models and can be seen in Figure 20 below.

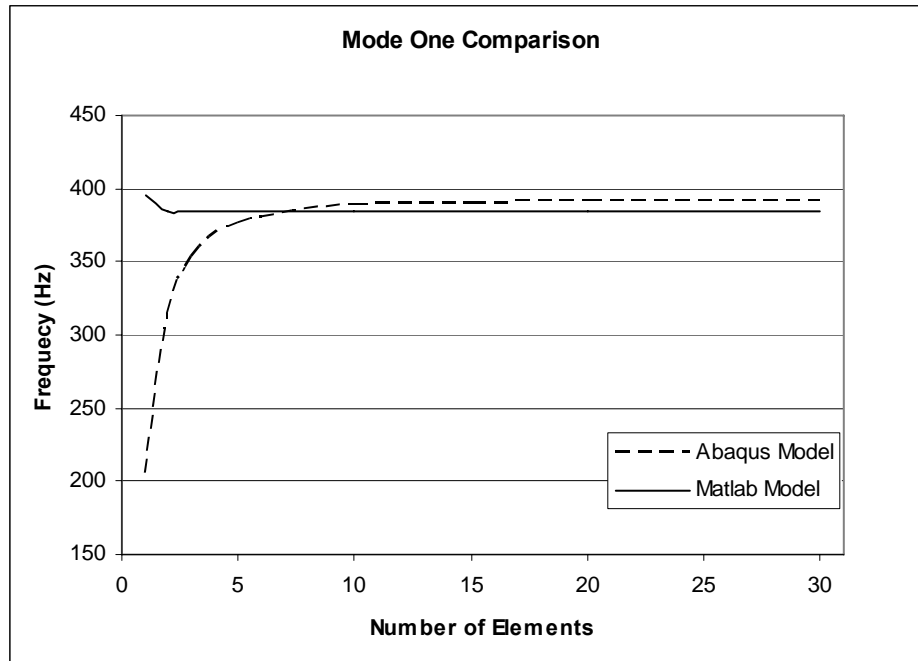


**Figure 20. Mode One Comparison**

It should be noted in the above comparison, the models converge at a mesh size of approximately 15 nodes. Though both models converge, they converge to different values. The first mode in both models produce relatively consistent results (1.8% difference) and it can be assumed that this value can be used as a baseline for the other Abaqus models. Once the beam element was created in both Abaqus and Matlab as a baseline for the other models, a plane stress, plane strain and a plate analysis were all completed for the homogeneous model to study the differences in the three modeling techniques.

The plane stress and plane strain both allowed the study of the internal workings of the beam as they were a side view of the beam as seen in Figure 21 below.

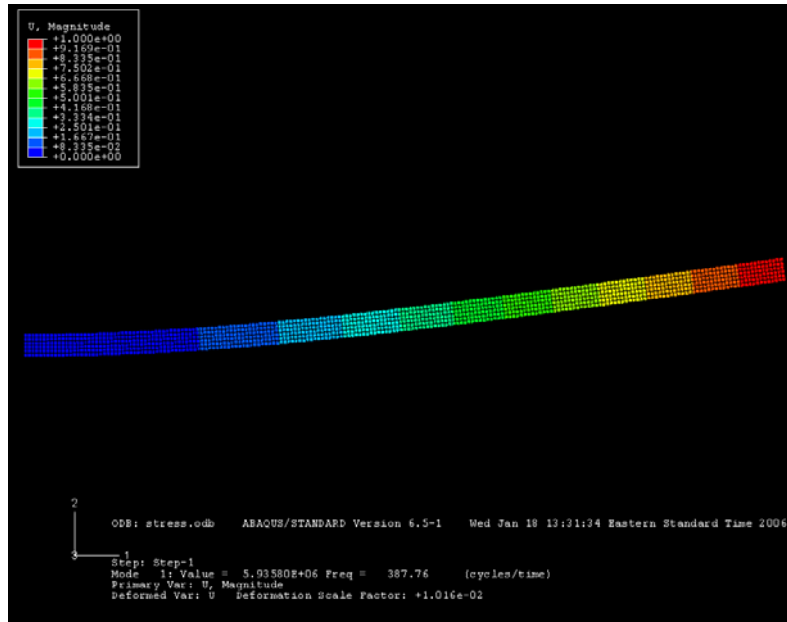


**Figure 21. Plane Stress/Strain Model**

The plane stress analysis treats the beam as extremely thin (into the page). This means that the beam has no width and hence no stress in the width direction, where in reality the width of the beam is 2.54cm. This means there would be some stress present in the width direction of the beam and therefore the model is not ideal. The plane strain analysis treats the beam like an infinite width plate with no strain into the page. This analysis also does not accurately capture the actual beam as the width is much less than ten times the length (a rule of thumb for determining a plain strain situation). Both of these analyses were used to model the FGM and were compared with the experimental results in the Analysis and Results section that follows. It was determined that in order for the solution to converge, the model needed to have at least 800 elements in the length direction (using square elements). Convergence was assumed when the first three natural frequencies changed less than one percent when doubling the number of elements in the model. Also it should be noted that when the model had only one element in the

thickness direction (Figure 22) as compared with two elements (Figure 23) there was a 92% change in the values for the first three modes. When the number was increased from two elements to three elements the change in the first three natural frequencies was reduced to 8%. Thus it is of great importance to include a minimum of two elements in the thickness direction.



**Figure 22. One Thickness Element**



**Figure 23. Two Thickness Elements**

The plate analysis was useful for determining the frequencies of the beam and the external stress concentration as the model did not assume a generic width as did the plane stress/strain analyses. Though, the model did not provide a view of the inside of the beam as seen in Figure 24 below and therefore the stress concentrations throughout the thickness were not visible.

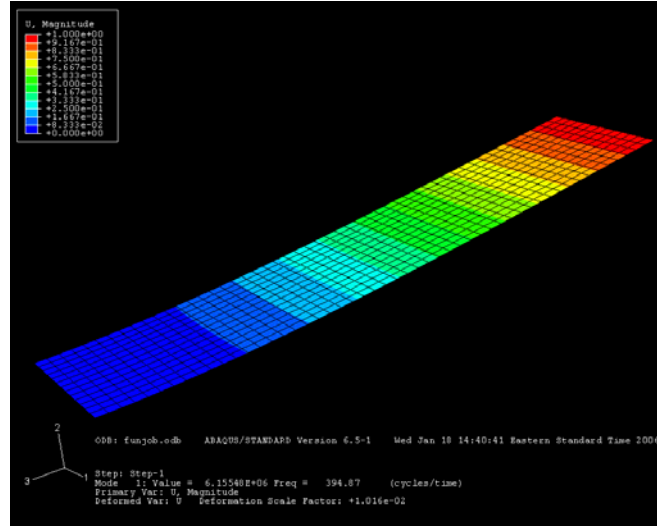


**Figure 24. Plate Model**

The plate provides much quicker convergence to a final value for the natural frequencies. The solution converges when the mesh has only 50 nodes along the length of the beam, as compared with 800 in the plane stress/strain analysis. The values for the homogeneous material's natural frequencies are compared with a plate composite representing the FGM and the actual test results in the Analysis and Results section of this thesis.

Once the homogenous material was modeled in each of the three cases above, it was modeled as 'functionally graded' but with homogeneous material properties to insure that the method for dividing the sections of the beam was valid. For both the plane stress and plane strain analyses, the thickness was divided up into sections according to the manufacturer's specifications as seen in Table 1 above. Once the specimen was divided, all of the individual sections or layers were all appointed the same material properties (that of the 85% TiB 15% Ti as seen in Table 2 above). The dimensions for the model were the same as those in the previous studies. See the model divisions in Figure 25

below. This figure represents the material as a true FGM with variations in materials, but for this study all layers are composed of the same material as stated above.

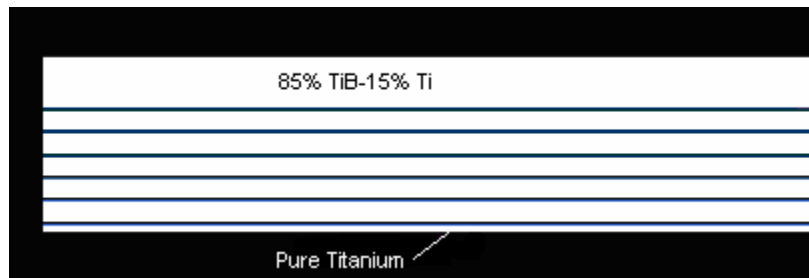


**Figure 25. FGM Ply Lay-Up**

As a result of the study completed previously to determine an appropriate size mesh for the plane stress/strain analysis, only a model with 800 elements along the length was examined. The 800 square elements allowed for at least two elements in every layer of the beam including the 0.2032mm bottom layer. It was found that the homogeneous division of the beam yielded results within five thousandths of a percent from the previous homogeneous models without layer divisions for both the plane stress and plane strain analysis. This verified that the method used to divide the beam into layers produced accurate results.

Once the accuracy of this method was determined the individual material properties for each of the actual FGM layers were entered into the Abaqus model. The model was run with 800 elements and then again with 1600 elements for the plane stress analysis. The results varied only seven one hundredths of a percent between the runs, so it was assumed that 800 elements was sufficient to produce accurate results (the values changed less than 1%). Results were obtained for both plane stress and plane strain and were compared with the experimental results in the Analysis and Results section of this thesis.

The plate was divided up into sections in a slightly different manner. Instead of creating a homogeneous cross section, a composite section was defined for the plate. Then each layer's material properties were entered along with the dimensions and orientation of the material (all layers having the same orientation of zero). This created a functionally graded section and the same properties and dimensions were entered as in the above study. Because of the nature of the plate, it was not possible to see the divisions of the cross section as in Figure 25 above, but the computer model that the program used assumes the same lay-up as the visual representation depicts above. The values obtained by the homogeneous 'FGM' using the composite lay-up yielded results within five hundredths of a percent from the original homogenous model when 50 elements along the length were used. This again verified that this method used to functionally grade, or set up divisions within, the material also produced accurate results.

Once this beam was verified the material properties from Table 2 were entered into the composite to create the FGM. The results from the run can be seen with the results from the plane stress and plane strain FGM results in Table 4 below.

**Table 4. Abaqus FGM Comparison**

<b>Model</b>	<b>Mode 1 (Hz)</b>	<b>Mode 2 (Hz)</b>	<b>Mode 3 (Hz)</b>
<b>Plane Stress</b>	314.7	1964.0	5463.4
<b>Plane Strain</b>	325.6	2031.6	5649.9
<b>Plate</b>	317.9	1983.8	5534.0

It should be noted that the plane stress analysis produced the lowest values for each of the modes while plane strain produced the highest. The plate produced results closer to the plane stress analysis than the plane strain analysis.

In order to examine the effects of the oscillations on the internal structure of the specimens, a stress analysis was required. The stress concentrations present in the beam were found by applying a sinusoidal forcing function to the tip of the beam. The periodic function used a Fourier series sine wave approximation with all of the cosine terms set equal to zero. The period function is capable of creating any shape function that can be constructed using Fourier series. The amplitude for the forcing function was set equal to one, and the model was run. Once the results were produced by Abaqus, a pictorial representation of the stress concentrations was displayed. The Von Mises stress, maximum principle stress, the normal and shear stresses were all found using Abaqus. Von Mises stress is usually used to determine the yield criteria for ductile materials and the material being studied was quite brittle. Therefore, the Von Mises stress did not prove to indicate the failure of the specimen analytically. The normal and shear stresses were combined in the maximum principle stress which occurred on a plane slightly inclined with respect to the length direction. The maximum principle stress was the highest stress value and was used in the analysis to determine when failure occurred. Also, a report was generated which included all of these specific values for every node in the beam's mesh. In order to find the specific points of interest it was necessary to display all of the node labels on the beam as seen for the top edge of the beam at the cantilevered end in Appendix C. The maximum stress occurred in the beam on the upper surface near the support as seen in Figure 26 below.

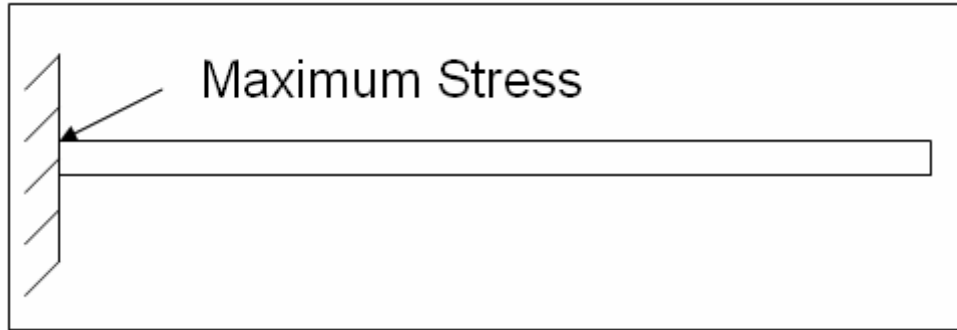


**Figure 26. Maximum Stress Location**

Once the node number was identified in Appendix C for the point of interest on the beam as seen above, a report generated in Abaqus was used to determine the exact values for the various stresses at that point in the beam. Please see an example of this report in Appendix B. The maximum stress occurred on the upper surface of the beam because of the variation in material properties throughout the thickness as depicted in Figure 27 below. The red coloring is the highest stress concentration and the blue is the lowest.

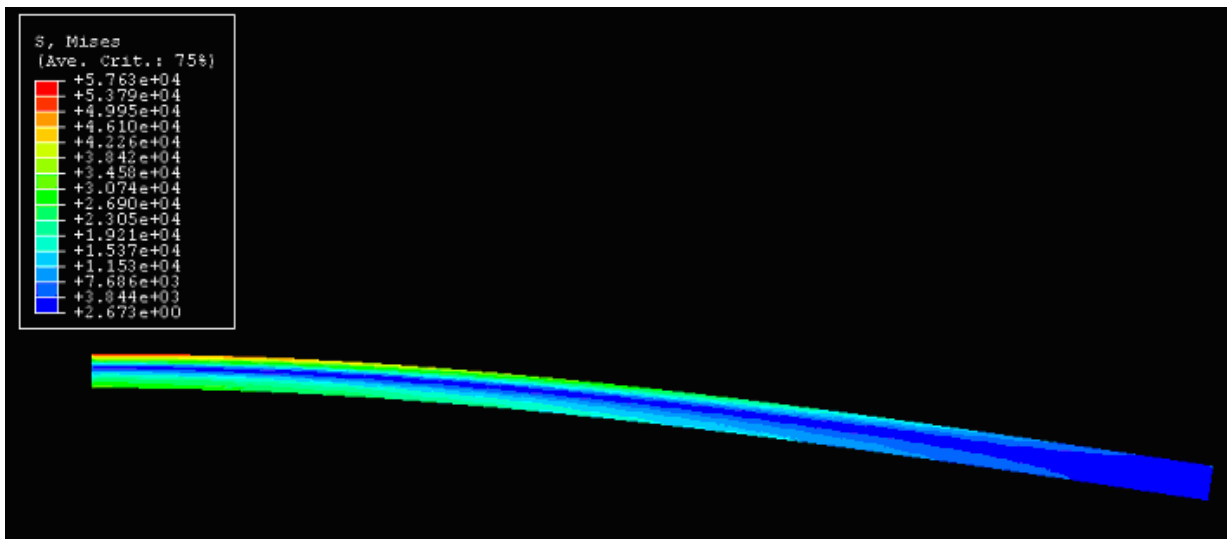


**Figure 27. Stress Concentrations**

This makes physical sense as one would expect the highest concentration to be present at the root of the beam, nearest the cantilevered support. For a homogenous beam the stresses are symmetric and the magnitude of stress in both the upper and lower surfaces would be the same, but because of the functional grade of the material properties the highest stress is present at the top left corner of the beam. The magnitude of the stress corresponds with the amplitude of one Newton for the forcing function. Stress is directly proportional to the force applied to the beam, so this ratio was used to find the amplitude of force necessary to reach the ultimate strength of the upper layer of the beam. This represented the load required to fail the beam with one cycle of a sinusoidal input. The lower portion of the beam was also examined, but it was determined that the magnitude of the force required could not be reached because the upper surface would fail before the stress required to fail the lower surface was achieved.

## **Summary**

FGMs are a type of composite material that combines different materials according to a function through the thickness of the material. In theory, the material properties are such that the material has both the positive thermal characteristics of the ceramic and the structural integrity of the metal component without a single drastic change in material properties which leads to stress concentrations and the failure of the component. There are many methods used in industry to create FGMs, but most are manufactured with discrete steps instead of a continuous function such as the theory suggests. The numerous discrete steps allow the material properties to change gradually enough to simulate a true smooth function.

The experimental procedures allowed for a verification of the manufacturer's specifications as well as provided a comparison for the Abaqus finite element results. Matlab was used as a method of verifying results from Abaqus. Once the model was baselined and it was certain that the results produced in Abaqus for the beam element were correct, several other models were created. These models allowed for the comparison with actual experimental data to help determine the material properties. Once the material properties were verified, an Abaqus simulation of a cyclic loading forcing function was performed to examine the through-the-thickness stresses within the specimens.

### **III. Analysis and Results**

#### **Chapter Overview**

This chapter discusses the results of the experiments and analyses performed in this research. First the experimental results are examined along with a statistical analysis to determine the validity of the data. The results from the Matlab finite element program are compared with the experimental results. Then the analysis performed in Abaqus is examined and compared with the experimental data to help determine the validity of the material properties found by Hill and Lin. Finally, the results for the through-the-thickness stress analysis are discussed.

#### **Experimental Results**

The experimental portion of this study included four major areas for the purpose of characterizing the FGM. These areas of experimentation were a static modulus of elasticity test and a frequency test which helped characterize the material properties. Also, experimental densities were found along with the damping of the specimens. Finally a study was done of the microstructures of the material using an optical microscope as well as a scanning electron microscope to examine a fracture surface.

##### ***Static Experiment Results.***

The results of the static analysis for the homogeneous material (85% TiB-15% Ti) can be seen in Figure 28 below.

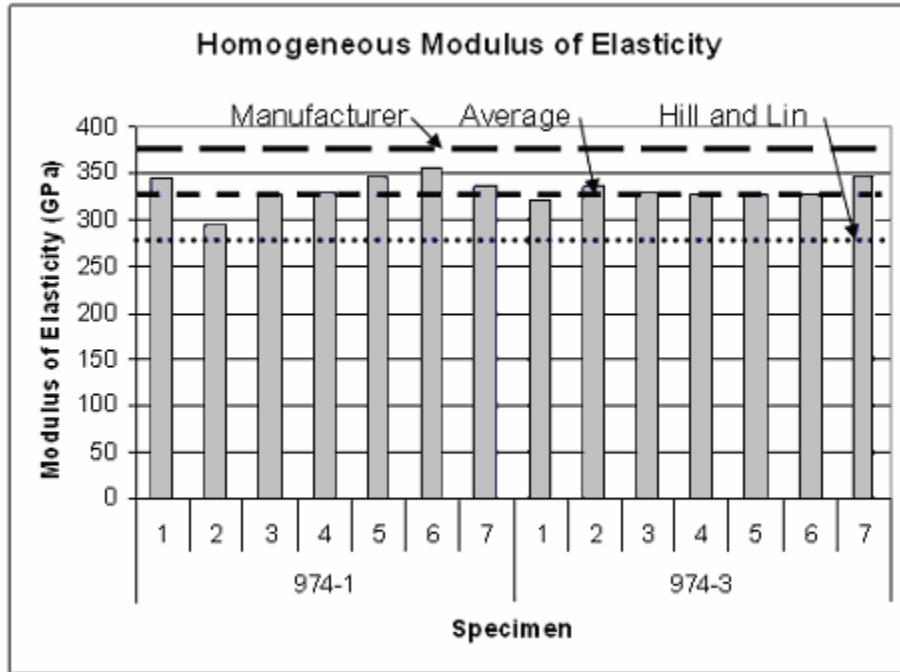


**Figure 28. Homogeneous Material Modulus of Elasticity Results**

The results are grouped by specimen number and the sheet of material from which the specimen was cut. The specimens' modulus of elasticity varies from a low value of 293.3 GPa to a high value of 345.9 GPa with an average value of 332.9 GPa. The modulus of elasticity for this material, found in the experimentation of Hill and Lin, was 274.3 GPa which was lower by 17.6%. The values provided by the manufacturer can be seen in Table 5 below [18].

**Table 5. Manufacturers Specifications**

% TiB	Modulus of Elasticity (GPa)
85	370.6
75	335.4
60	280.9
45	227.9
30	180.6
15	142.9
0	119.0

It should be noted that these values required interpolation into the form seen above as the manufacturer did not provide values for the volume increments present in the FGM. It was unknown how they tested this material to produce these results. It was assumed that the manufacturer produced homogeneous specimens of each composition for testing, and it was possible that the material properties could have changed significantly when the material was made *in situ*. When interpolating the values from the data provided by the manufacturer, the average value for each composition was found and plotted as seen in Figure 29 below.

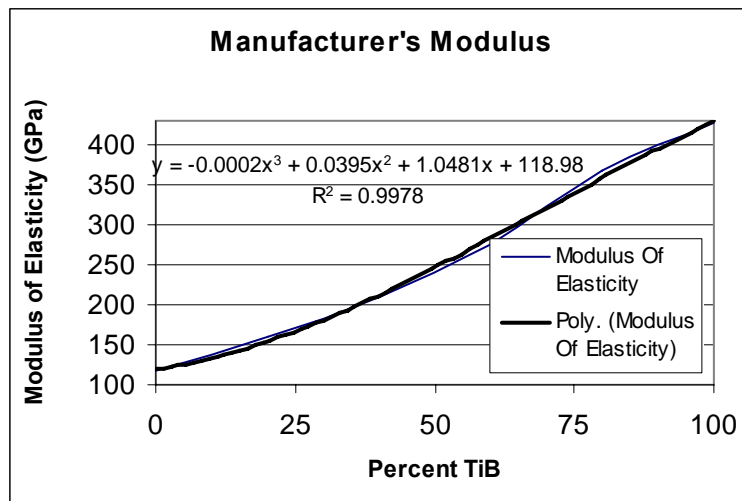


**Figure 29. Specifications Interpolation Chart**

Once the values were plotted a third order polynomial trend-line was added along with the equation for the polynomial. The equation was then used to solve for each individual layer used in the actual FGM (see Table 5 above). According to the equation the value for the 85% TiB-15% Ti homogeneous material was 370.63 GPa which was 11.3% higher than the measured experimental value and 35.1% higher than the values found by Hill and Lin. There was a large disagreement between the three methods of finding the modulus of elasticity. All three methods were modeled in Abaqus and compared to the dynamic test results to help determine the most accurate specifications for the modulus.

A statistical analysis was completed to determine if the modulus of elasticity varied from sheet to sheet. The Student's  $t$  distribution was used to find the variance between the samples of data. This method used the same standard deviation for both samples and since both samples did not already have the sample standard deviation an estimator was used and can be seen in the equation below [15].

$$s^2 = \frac{\sum_{i=1}^{n_1} (y_i - \bar{y}_1)^2 + \sum_{i=1}^{n_2} (y_i - \bar{y}_2)^2}{n_1 + n_2 - 2} \quad (17)$$

In this equation,  $s$  is the *standard deviation*;  $n_1$  and  $n_2$  are the *number or samples* in each sheet of material. The individual value for the *modulus of elasticity* is represented as  $y_i$  for each sample and the *mean value* for each is designated as  $y_1$  bar and  $y_2$  bar. Once a value for the overall standard deviation estimate was achieved, the *test statistic*,  $t$ , was solved for using equation 18 below [15].

$$t = \frac{(\bar{y}_1 - \bar{y}_2)}{s \sqrt{\frac{1}{n_1} + \frac{1}{n_2}}} \quad (18)$$

The value for  $t$  was then compared with a tabulated  $t$  value based on the number of degrees of freedom for the system which is defined as  $n_1 + n_2 - 2$  [15]. The value for  $t$  found using the equations above was 0.341 and the tabulated value for  $t$  at a confidence interval of 90% was 1.356. This means that one can infer that the mean of each specimen was the same to a confidence 90%.

The results for the FGM static modulus test produced a similar distribution of values and can be seen in Figure 30 below.

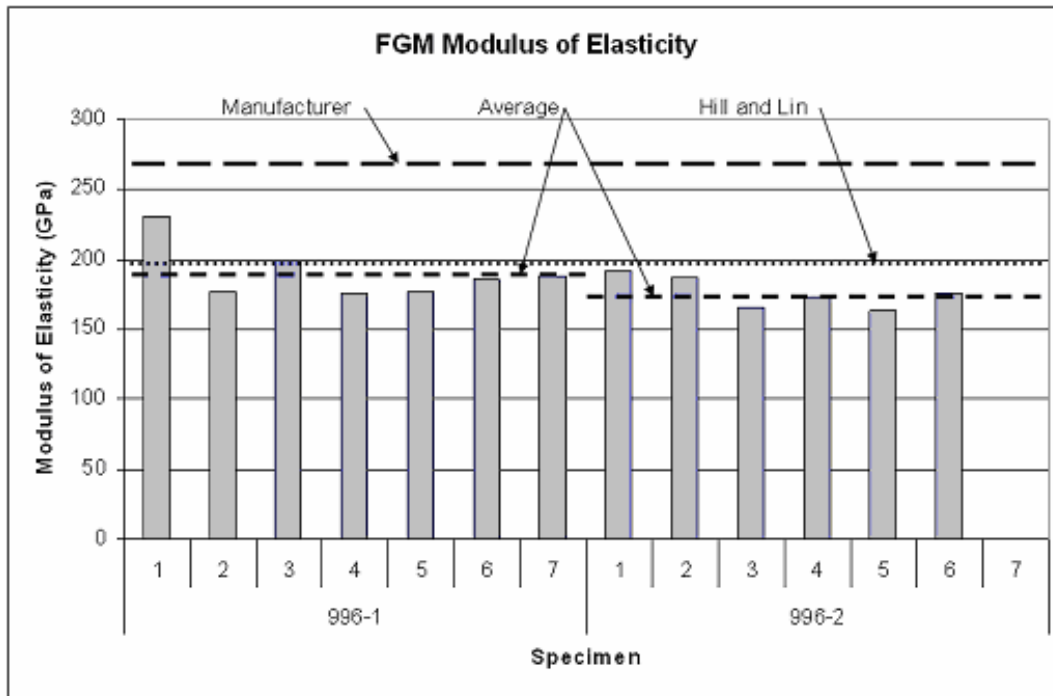


**Figure 30. FGM Modulus of Elasticity Results**

It should be noted that the specimens from the 996-1 sheet of material had a larger variation (standard deviation of 19.3) as compared with the specimens from sheet 996-2

(standard deviation of 11.2). Also the mean value for sheet 996-1 was 190.7 GPa compared to a value of 176.3 GPa for sheet 996-2. The same statistical analysis as above was performed on these two sheets of material to determine if the results were different between the sheets. The  $t$  value found using the data from the specimens was 1.599 while the  $t$  value from the tabulated data at a confidence interval of 90% and with 11 degrees of freedom was 1.363. This means that to a confidence of 90% the sheets from which the specimens were cut did in fact have different mean values. The average value of the modulus of elasticity for the FGM sheet 996-1 varied from the Hill and Lin theoretical value of 198.5 GPa by 4.1% while sheet 996-2 varied by a value of 12.6%. The theoretical value for the average modulus of elasticity, using Hill and Lin's specifications, for the cross section of the FGM was found by summing the individual layer properties multiplied by their thickness and then dividing by the thickness of the entire beam. Both FGM sheets were below the values provided by Hill and Lin while both of the homogeneous sheets were above the theoretical values. The data from sheet 996-1 was the closest to the theoretical results (4.1% difference) and the difference between sheets is large enough to assume that specifications found by Hill and Lin are a close approximation to those of the actual material. The specifications from the manufacturer indicate an average modulus of elasticity of 266.78 GPa which is 39.9% higher than the experimental values for sheet 996-1 and 51.3% higher than sheet 996-2. Hill and Lin's specifications according to this study are the closest approximation to the experimental results. The theoretical values found by Hill and Lin were much closer for the FGM than for the homogenous material. This difference could be due to the fact that the values that Hill and Lin found were from experimentation on FGM specimens and not

from a homogenous material as was tested in this study. This would imply that the manufacturing process used for creating the FGM slightly alters the material properties as each of the layers is slightly mixed with the surrounding layers due to the high temperatures used when manufacturing each layer *in situ*. This also suggested that the rule of mixtures did not work ideally and further testing should be completed beyond the interpolation of the rule of mixtures to determine the material properties of the FGM. The modified rule of mixtures equation as discussed in the FGM Theory section above was not able to be used for this material because the empirical parameter  $\bar{A}$  was not available for this material. Hill and Lin produced similar results within the FGM which were confirmed in the dynamic tests as the best theoretical values to be used in Abaqus to model the material.

#### ***Dynamic Test Results.***

The dynamic test was performed to examine the natural frequencies of the specimens, which in turn helped verify the material properties as well as provided a comparison for the Abaqus finite element models. The output of the dynamic test for specimen one, sheet 974-1, can be seen in Figure 31 below. This specimen was cantilevered directly to the table as seen in Figure 11 above.

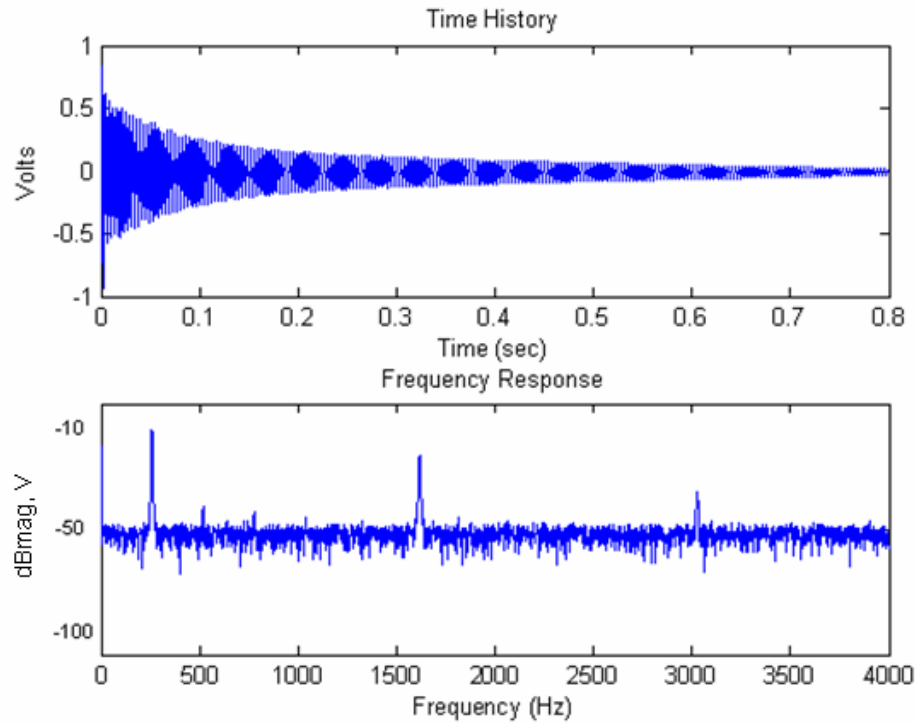


**Figure 31. Sample Matlab Plot (974-1 #1)**

This run was completed with a resolution of 3200 data points over a range of 4000 Hz so only the first two bending modes can be seen. Once plots such as this were produced for all of the tested specimens the values at the peaks of the frequency plot were determined to be the bending modes. The time domain allowed one to see the decay of the beam. In this case the first two bending modes were 257.5 Hz and 1613.8 Hz. The third mode of the beam which was a torsion mode (and will be ignored in this thesis) was visible at around 3000 Hz. The third bending mode required a lower resolution run and for this specimen occurred at a value of 4290 Hz. The results from all of the specimens tested can be seen in Table 6 below.

**Table 6. Dynamic Test Results**

<b>Material</b>	<b>Sheet</b>	<b>Specimen</b>	<b>Mode 1 (Hz)</b>	<b>Mode 2 (Hz)</b>	<b>Mode 3 (Hz)</b>
<b>FGM</b>	<b>996-1</b>	<b>1</b>	202.5	1318.8	3570
		<b>2</b>	287.5	1828.8	5170
		<b>4</b>	283.8	1802.5	5080
	<b>996-2</b>	<b>1</b>	198.8	1273.8	3540
		<b>2</b>	291.3	1892.5	5340
		<b>4</b>	285.0	1773.8	4920
<b>Homogeneous</b>	<b>974-1</b>	<b>1</b>	257.5	1613.8	4290
		<b>4</b>	387.5	2423.8	6860
		<b>7</b>	386.3	2420.0	6820
	<b>974-3</b>	<b>1</b>	256.3	1615.0	4360
		<b>4</b>	392.5	2450.0	6860
		<b>7</b>	388.8	2426.3	6860

The values for the first specimen in each sheet were much lower than the other values because they were 2.54 cm longer than the other specimens. The experimental results were compared with these experimental results in the Abaqus Frequency Results section below. Each specimen had slightly different dimensions as well according to Table 7 below.

**Table 7. Test Specimen Dimensions**

<b>Material</b>	<b>Sheet</b>	<b>Specimen</b>	<b>Length (cm)</b>	<b>Width (cm)</b>	<b>Height (cm)</b>
<b>FGM</b>	<b>996-1</b>	<b>1</b>	12.70	2.460	0.319
		<b>2</b>	10.16	2.379	0.312
		<b>4</b>	10.16	2.357	0.310
	<b>996-2</b>	<b>1</b>	12.70	2.593	0.321
		<b>2</b>	10.16	2.351	0.315
		<b>4</b>	10.16	2.374	0.311
<b>Homogeneous</b>	<b>974-1</b>	<b>1</b>	12.70	2.351	0.315
		<b>4</b>	10.16	2.433	0.315
		<b>7</b>	10.16	2.464	0.315
	<b>974-3</b>	<b>1</b>	12.70	2.396	0.316
		<b>4</b>	10.16	2.446	0.314
		<b>7</b>	10.16	2.459	0.316

The differences in dimensions contributed to the differences in natural frequencies as natural frequencies were highly dependent on the dimensions of the specimen. The height of each specimen affected the natural frequency the most because that dimension was cubed in the formula for the second moment of inertia which impacted the theoretical natural frequency. It should also be noted that the specimens used in the test included the long piece cut perpendicular to the sheet of material as seen in Figure 10 above as well as a center specimen (number four) and an outside specimen (number two for the FGM and number seven for the homogeneous). The reason two different outside specimens were tested was because the seventh specimen on one of the FGM sheets was shipped broken. Also, the length of each specimen was measured from the edge of the cantilevered support.

When comparing the modulus of elasticity results for the FGM from Figure 30 above with the dynamic results from Table 6 it should be noted that the modulus of elasticity was much greater for specimen 996-1 number one when compared with 996-2 number one. This corresponded to higher natural frequencies for the stiffer specimen (996-1 number one). Also notice that when comparing the dimensions for the same specimens, 996-2 number one had a larger width and height (2.593 cm x 0.321 cm compared with 2.460 cm x 0.319 cm). This suggested that the 996-2 specimen should have larger natural frequencies than the 996-1 specimen if each had the same modulus of elasticity. This information confirmed that the specimens did in fact have variations in the modulus of elasticity which suggested an imperfect manufacturing process. This variation also introduced variation and error into the modeling of the specimens in Abaqus.

Due to the fact that all of the specimens had slightly different dimensions as well as natural frequencies, the average dimensions for the similar specimens (the longer specimens were excluded) as well as the results for the frequency analysis are shown in Table 8 below. This table provides a baseline for the Abaqus analysis which was used to model these average specimens.

**Table 8. Average Dimensions and Natural frequencies**

<b>Material</b>	<b>Average Dimensions (cm)</b>			<b>Average Natural Frequencies (Hz)</b>		
	<b>Length</b>	<b>Width</b>	<b>Height</b>	<b>Mode 1</b>	<b>Mode 2</b>	<b>Mode 3</b>
<b>FGM</b>	10.1600	2.3651	0.3121	286.9	1824.4	5127.5
<b>Homogeneous</b>	10.1600	2.4505	0.3150	388.8	2430.0	6850.0

The mass of each specimen was measured on a digital scale and then divided by the volume. The average densities are shown in Table 9 below. They were compared with the theoretical values found by Chandran, Panda and Sahay through their research of this material [2]. The data they provided included only the density of pure TiB and Ti, so in order to determine values for the entire cross-section an interpolation was required. Once the data was interpolated, the average value was found for the theoretical material to compare with the average value measured for the actual FGM specimens.

**Table 9. Density Comparison**

<b>Material</b>	<b>Measured Density (Kg/m<sup>3</sup>)</b>	<b>Theoretical Density (Kg/m<sup>3</sup>)</b>	<b>% Difference</b>
<b>FGM</b>	4515.797	4564.6	1.1
<b>Homogeneous</b>	4683.785	4561.5	2.6

It can be seen that the differences in density are relatively small. Surprisingly the density for the homogenous material had a larger percent difference than the FGM. One would assume that it would be easier to predict the density for a homogeneous material, but that was not the case in this study. Different densities corresponding to both

theoretical and measured values were used in the Abaqus analysis, which follows in the Abaqus Frequency Results Section, to study the effect of the density on the natural frequencies.

The same dynamic test as above was performed on one set of homogenous specimens with a different method of clamping the specimens as discussed in the Experimental Setup and Procedures above. This study was completed to examine the effects of the clamping method on the results of the experiment. The results for the first mode of the vertical post clamp are compared to the results from the table clamp in Table 10 below.

**Table 10. Clamp Method Comparison**

<b>Sheet</b>	<b>Specimen</b>	<b>Table Clamp Mode 1 (Hz)</b>	<b>Vertical Post Clamp Mode 1 (Hz)</b>	<b>% Difference</b>
<b>974-1</b>	<b>1</b>	257.50	256.25	0.49
	<b>4</b>	387.50	380.00	1.94
	<b>7</b>	386.25	378.75	1.94

The results show that the vertical post clamp produced results that were consistently lower than that of the table clamp. Because the same specimens were used, the dimensions of each specimen were identical along with the modulus of elasticity. This shows that the clamp itself accounts for the difference in the natural frequencies. Therefore it is important to use a clamping method which secures the specimen with as little extra structure as possible as that structure can contribute to frequencies produced by the experiment. In this study this was accomplished by bolting the specimen directly to the optical table as opposed to using a more elaborate clamping method which introduced a source of error into the results.

### ***Damping Results.***

Another study was performed using the data from the experimental frequency tests. This included finding the damping coefficient for the material. This study was completed in order to further characterize the FGM as well as aid in the future study of this material to include cyclic loading tests, for which the damping coefficient is beneficial. The damping coefficient is a useful term in monitoring the damage accumulation for a specimen under cyclic loading. It allows one to predict the failure in the specimen during a fatigue test. The damping coefficient was found using the logarithmic decrement method. The method involved identifying the peak values in the time history output as depicted by the graph in Figure 32 below.

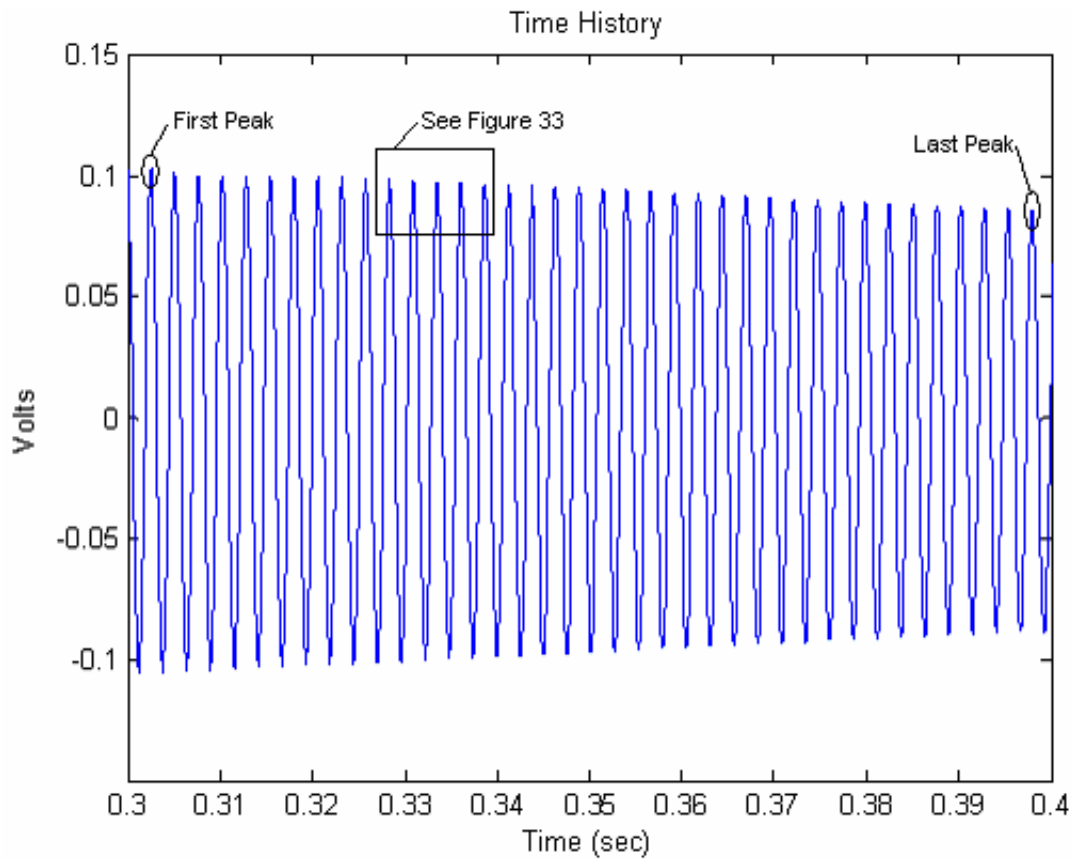


**Figure 32. Damping Coefficient Time History**

This graph shows the time history for specimen 974-1, number four, for a period of 0.1 seconds in the steady state portion of the oscillations. Once a peak was identified in the graph the specific value was found in the raw data for each specimen according to the time at which the peak occurred. The peaks were then counted to determine the number of oscillations the beam had made in the time period of 0.1 seconds and then the value for the final oscillation was found in the raw data in order to obtain the best accuracy possible for the values of the peaks. The *decrement*,  $r_n$ , is defined by the relationship seen in equation 19 below [3].

$$r_n = \frac{x(t)}{x(t + nT)} \quad (19)$$

Where  $x(t)$  is the *voltage* at the first peak,  $x(t + nT)$  is the *voltage* at an *integer number*,  $n$ , of *periods*,  $T$ , from the original peak. The value for  $n$  was found by counting the peaks in between the first and last peak examined. Once a value for the decrement was found, the equations below were used to determine the damping of the beam [3].

$$\alpha = \frac{1}{2\pi n} \ln(r_n) \quad (20)$$

$$\zeta = \left( \frac{\alpha^2}{1 + \alpha^2} \right)^{1/2} \quad (21)$$

Where  $\zeta$  is the damping coefficient. It should also be noted that for small damping  $\zeta \approx \alpha$ . The results for the specimens can be seen in Table 11 below.

**Table 11. Experimental Damping Coefficient**

<b>Material</b>	<b>Sheet</b>	<b>Specimen</b>	<b>Damping Coefficient</b>	<b>Average Value</b>
<b>FGM</b>	<b>996-1</b>	<b>1</b>	0.0034	<b>0.0016</b>
		<b>2</b>	0.0008	
		<b>4</b>	0.0007	
	<b>996-2</b>	<b>1</b>	0.0010	<b>0.0015</b>
		<b>2</b>	0.0015	
		<b>4</b>	0.0021	
<b>Homogeneous</b>	<b>974-1</b>	<b>1</b>	0.0015	<b>0.0010</b>
		<b>4</b>	0.0008	
		<b>7</b>	0.0007	
	<b>974-3</b>	<b>1</b>	0.0014	<b>0.0011</b>
		<b>4</b>	0.0011	
		<b>7</b>	0.0008	

It can be seen that individual values varied considerably, but the values obtained by the average for each sheet provide an estimate for the specimens in a cantilevered support. Although a large portion of the damping coefficient was attributed to the clamping method, this study provided an estimate for the damping under similar clamp conditions. These values should not be taken to be the true damping coefficients for the material, as that would require the specimens to be tested while suspended in a vacuum. These values were intended to provide an approximate damping coefficient for the system, which will be useful in cyclic loading tests as discussed above which make use of a similar clamping method. Some of the error in the reading was due to the fact that the sample rate did not allow for data to be taken at the exact physical peak of each oscillation of the beam. Often the sample was taken slightly below the physical peak or considerably below the peak as the following oscillation produced a higher peak than the previous (a physical impossibility). This means that the peaks chosen for examination were most likely not true peak values for voltage, though the values produced did give a

reasonable estimate for the damping coefficient. The magnified view of the peaks in Figure 33 (magnified from the time history plot of Figure 32) below shows how the sample rate does not generate a smooth curve which is necessary to achieve the exact physical peak of the oscillation. It should be noted that the higher number of cycles examined in this study decreased the impact of this source of error and the values presented in Table 11 above can be assumed to be relatively accurate.

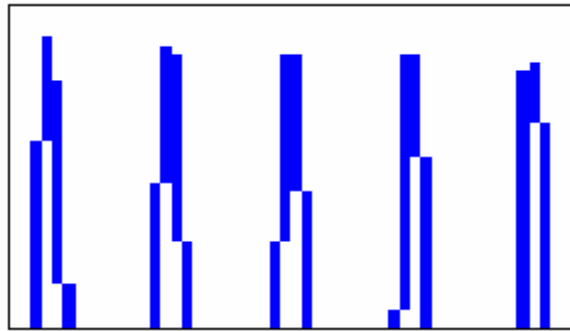


**Figure 33. Magnified Time History Peaks**

### ***Microstructures Results.***

The optical microscope was able to capture images which gave insight into the distribution of materials throughout the thickness. Figure 34 shows a side view of specimen number seven from sheet 996-1. Some of the layers can be seen clearly while other layers are quite difficult to distinguish. Division lines were overlaid on the photograph to help pick out the individual layers. Larger magnification may be needed in order to clearly identify each individual layer.

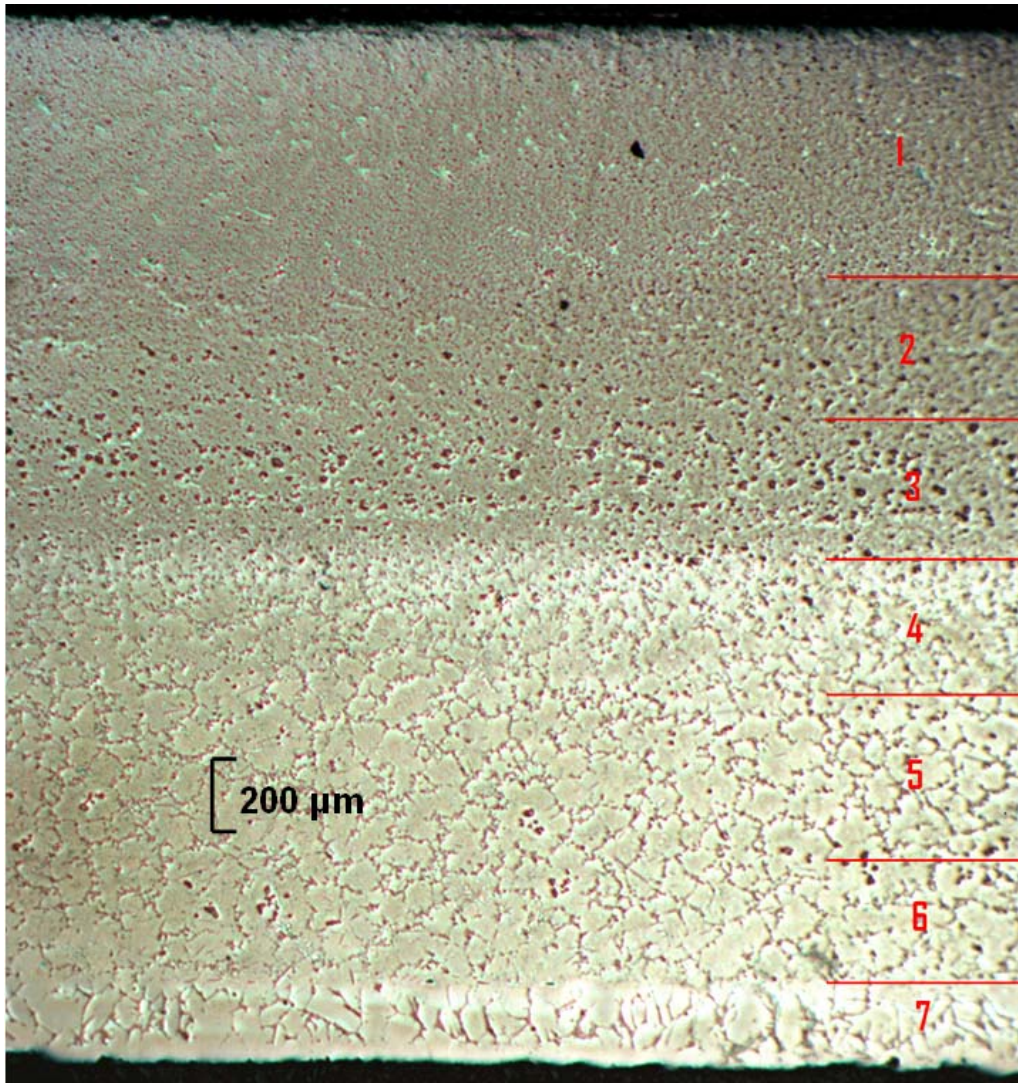


**Figure 34. FGM Side View**

The top layer shown in this photograph was 85% TiB-15% Ti and the bottom layer was the foil of commercially pure titanium. According to this photograph which had a magnification factor of 50X, it appeared that layer one was not quite as thick as the manufacturer's specifications suggested. It appeared that layer one was less than twice the thickness of the middle layers. This is contrary to the specifications sent by the manufacturer which stated that layer one was more than twice the thickness of the other layers (see Table 1). Also it appeared that layer five was slightly thicker than the other

middle layers. This was less clear because it was difficult to distinguish the separation between layers four, five and six. The manufacturer did mention in an e-mail [17] that layer one was probably a little thinner than the provided specifications and that layer six might be slightly thicker. This information helped to confirm the observations made pertaining to the first layer and suggested that the observations made about layer five could also be valid. Variations in layer thickness were studied in the Abaqus models (see Abaqus Frequency Results below) to determine the effect on the analytical models of changing layer thicknesses.

A higher magnification factor (200X) was used to examine the boundaries of the layers. Figure 35 shows the intersection of layer six and seven.

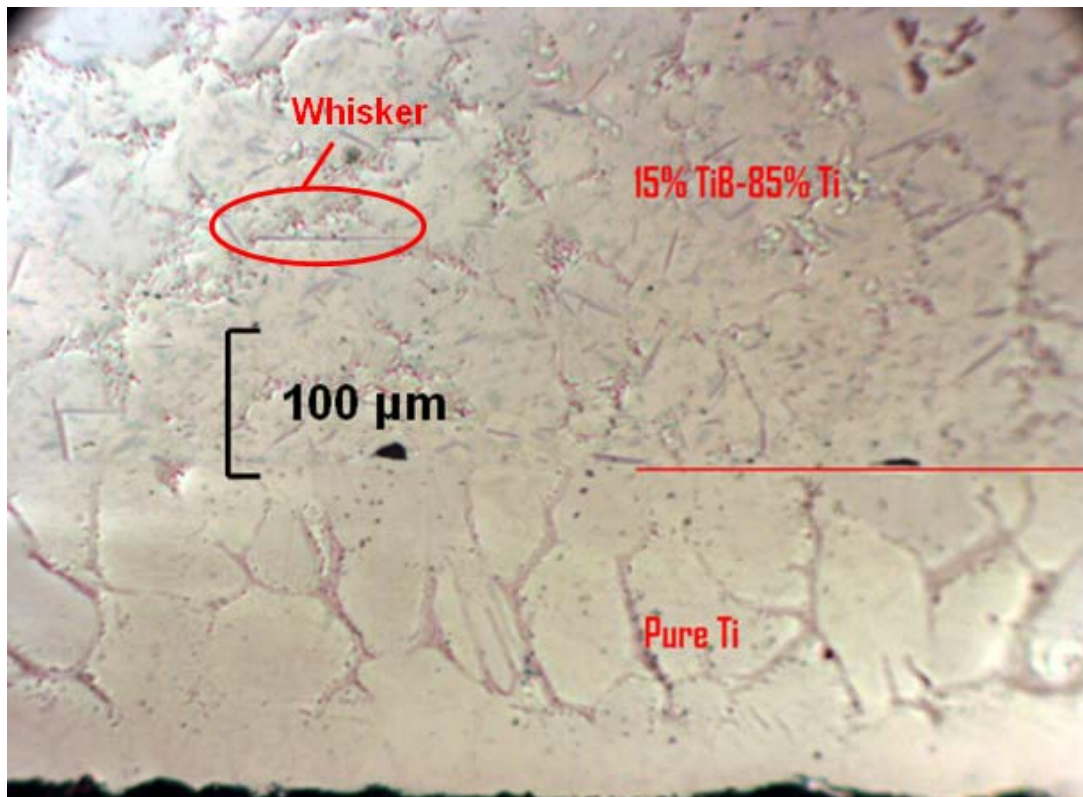


**Figure 35. Layer Intersection**

The holes present along the boundary should be noted. This could prove to be an important characteristic of this material or manufacturing process, as under cyclic loading these holes provide an excellent spot for crack initiation. A crack could easily form along this boundary line causing the material to fail. Another interesting observation was that whiskers were visible in the upper layer.

There was an opportunity to study the fracture surface because of the specimen being sent broken from the manufacturer. This became important to gain insight into the potential failure features of the material for future research. The future intent is to evaluate the fatigue properties of this particular FGM composition, and the method in which it fails will have an impact on interpreting the results from that experiment. In order to gain this understanding, the fracture surface from this specimen was examined under a scanning electron microscope (SEM) to determine how the part failed as well as to make observations about the characteristics of the fracture surface. Figure 36 is a photograph from the SEM with a low resolution (see scale in the figure), and shows the entire thickness of the fracture surface.

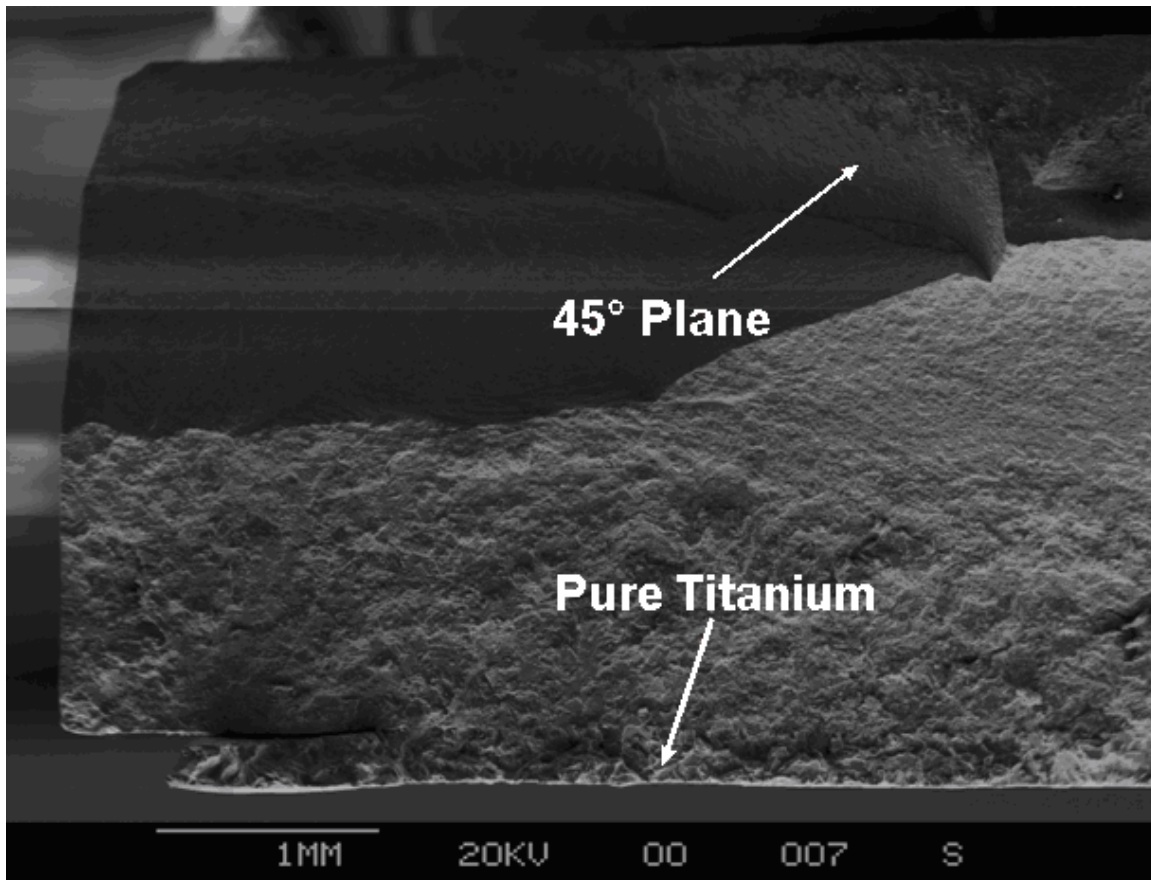


**Figure 36. Fracture Surface**

This photograph was taken with the pure titanium foil on the bottom. It should be noted that near the middle of the thickness the characteristics of the failure seem to change noticeably. The top is more of a smooth surface while the bottom half looks more textured. This is approximately the point at which the material transitions from majority titanium to a majority titanium-boride. Also, near the top of the figure a shear plane can be seen at a 45° angle to that of the rest of the fracture surface. This suggested that this portion of the material may have failed in a ductile manner as “shear stress dominates deformation and ductile fracture” [24]. This would have been the case if we knew that the material was pulled apart in pure tension. But because of the prior knowledge of the material properties, it was assumed that this material failed in a brittle fashion and

therefore the 45° plane becomes an insight into the method of failure. The specimen was most likely bent or twisted slightly to create a maximum tensile stress along that plane. This could be due to simply dropping the specimen, creating a moment in the beam which would produce the 45° plane as seen in the figure above. Finally this photograph shows that the titanium foil in the bottom left-hand corner chipped apart from the rest of the material (see enlarged version in Figure 37 below).

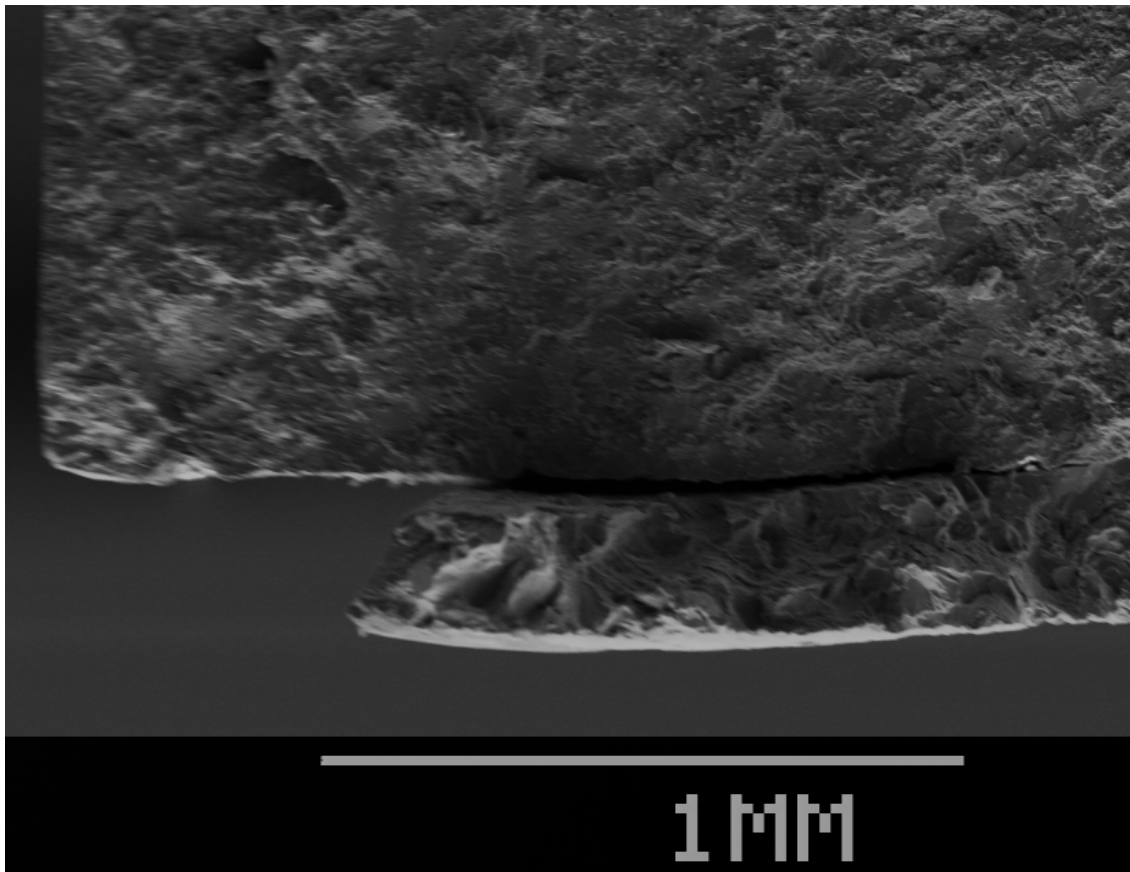


**Figure 37. Foil Separation**

This separation should be a concern for the operational use of this material. When FGMs are layered in discrete steps there is a chance that the layers will delaminate, or that failure will occur along these boundaries.

The upper surface which appears smooth in Figure 36 can be seen at ten times higher resolution in the SEM photograph in Figure 38 below.

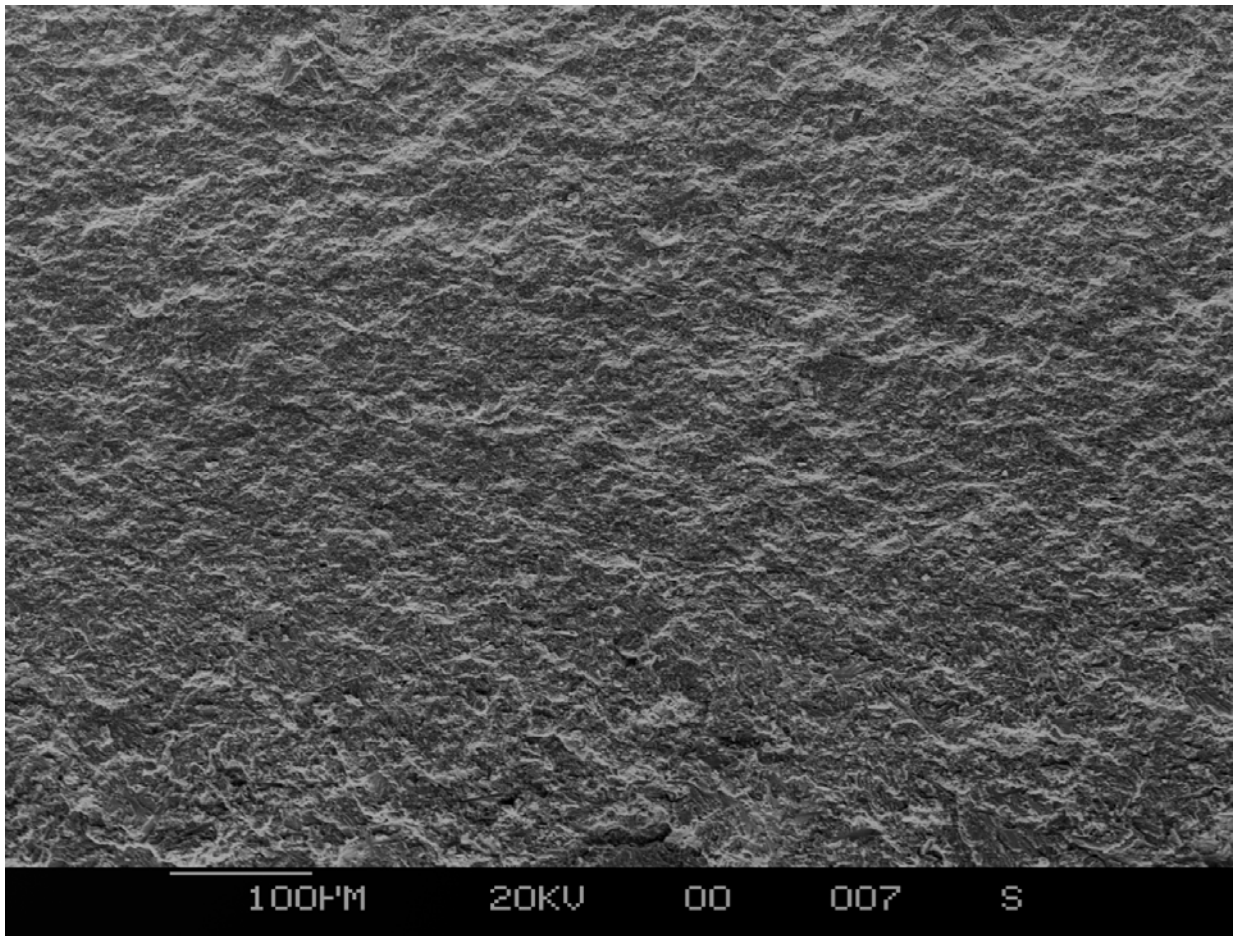


**Figure 38. Upper Fracture Surface**

The dimpled appearance suggested a ductile failure, but at closer inspection it was seen that these were not dimples. Dimples are the result of a metal stretching in an attempt to remain intact with the opposite side of the material and require high energy. This fracture surface was mostly ceramic which means that one would expect to see the opposite of dimpling or what would appear to be a bumpy surface. These two characteristics can be hard to distinguish, but because of the prior knowledge of the

material being examined it was inferred that this was a brittle failure of a ceramic material. The bottom portion of the fracture surface can be seen in Figure 39 below.

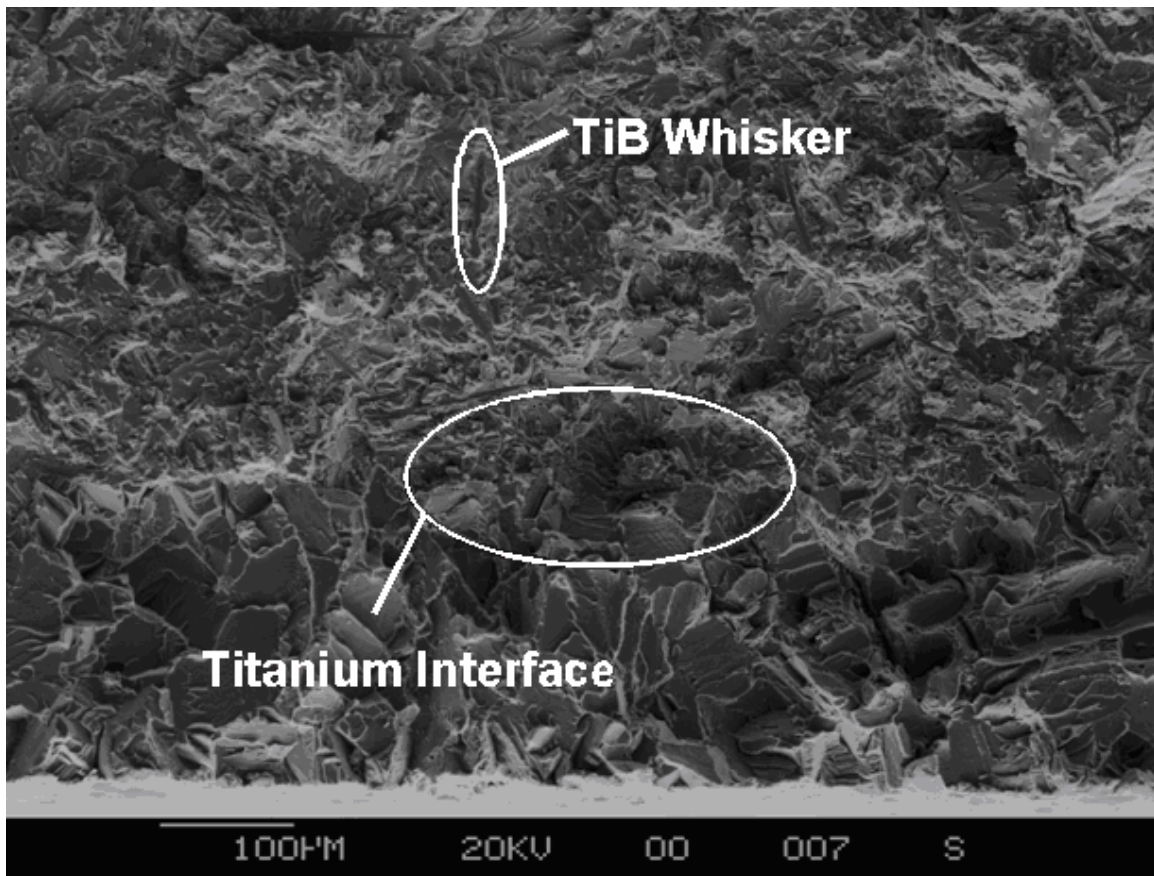


**Figure 39. Lower Fracture Surface**

This photograph showed a brittle mode of failure, as there was no pitting in the fracture surface. Also river marks on the fracture topography indicate a brittle failure. This is an interesting phenomenon because one would expect the titanium to fail in a more ductile manner. This brittle behavior could be due to the boron from the upper layers seeping into the titanium during the high temperature manufacturing process which drastically embrittles the titanium, according to materials scientist Dr. Stephan Russ of the Air Force Research Laboratory's Materials Directorate. This fact becomes important in the future research of this material as the titanium may not provide the fracture

toughness that it otherwise would in its more ductile natural state. This potentially hinders the positive structural characteristics that the titanium was intended to offer the FGM. The difference in the appearance across the thickness of the fracture surface did not indicate different failure characteristics but rather the differences in material properties. The entire cross section was determined to have failed in a brittle manner. Another interesting observation was that in this section the titanium foil had not delaminated. Also, in the upper portion of this photo the outline of whiskers can be seen. This observation should be compared to Figure 38 where there was a much higher percentage of TiB present, but none of the individual whiskers were visible. This was because the whiskers had turned into conglomerations of TiB due to the fact that the percentage of TiB was higher than that of titanium. Therefore, the fracture surface was actually splitting the conglomerations of TiB which make up the fracture surface.

### **Matlab Frequency Results**

The Matlab finite element program was created to verify that the results obtained in Abaqus were close to the actual results and to gain an understanding into the workings of the finite element method. Also, these values were used to compare with the experimental findings. The results for the Matlab finite element code for the first mode can be seen in Table 12 below.

**Table 12. Matlab Results**

<b>Number of Elements</b>	<b>Mode 1 (Hz)</b>
1	392.2
2	381.7
3	380.9
5	381.0
10	381.4
15	381.6
20	381.7
30	381.8

This data was generated using the average dimensions as seen in Table 8 above and using the material properties of the 85% TiB-15% Ti material seen in Table 2. This allowed the comparison with the results from the experimental tests. When compared with the experimental results, it was seen that mode one was 1.8 % lower. Although this model was relatively close to approximating the behavior of the model it was necessary for a more comprehensive analysis which could only be completed in a finite element software program like Abaqus.

### **Abaqus Frequency Results**

The first Abaqus test was to examine the homogeneous material, consisting of 85% TiB-15% Ti, which commercial FEA programs are able to model quite accurately. The homogeneous beam with the average dimensions as shown in Table 8 above was first modeled using a plane stress analysis. Different material properties were experimented with and compared with the experimental results. First the material properties found by Hill and Lin with the densities from Chrandran, Panda and Sahay were modeled (see Table 2 above). Next, the same specifications were tested with the experimental density,

and then the experimental density and modulus of elasticity found in the static experiment were both used. Finally the values provided by the manufacturer were used with both the experimental density and the density provided by Chandran, Panda and Sahay. The model progressively worsened with respect to the experimental values for the homogenous material, with each variation mentioned above. See the results for the plane stress model in Table 13 below.

**Table 13. Abaqus Specifications Comparison**

2-D Plane Stress	Hill-Lin E & Chandran $\rho$	% Diff	Hill- Lin E with Experimental $\rho$	% Diff	Experimental $\rho$ & E	% Diff	Manufacturer E with Experimental $\rho$	% Diff	Manufacturer E with Chandran $\rho$	% Diff
Mode 1 (Hz)	381.70	1.83	376.69	3.11	414.98	6.73	437.86	12.62	443.69	14.12
Mode 2 (Hz)	2382.20	1.97	2350.90	3.26	2589.90	6.58	2732.70	12.46	2769.10	13.95
Mode 3 (Hz)	6626.40	3.26	6539.30	4.54	7204.00	5.17	7601.30	10.97	7702.50	12.45

These values were all compared with the experimental results of 388.8 Hz for the first mode 2430 Hz for the second mode and 6850 Hz for the third mode as seen in Table 8 above. The conclusions from this study showed that based on the frequency results the best specifications for the model were those found by Hill and Lin in their research along with the densities provided by Chandran, Panda and Sahay. The specifications provided by the manufacturer were in fact the worst representation of the actual beam with the experimental results from the static and density tests about midway between the results of Hill and Lin and the manufacturer' specifications. All of the results were above the experimental results except for the Hill and Lin modulus of elasticity models. The experimental results should be lower than the theoretical results because of the imperfect clamping of the beam. With an imperfect clamp the natural frequencies decreased as

seen in the experiment above comparing the table clamp to the vertical post clamp. Also, the mass of the accelerometer could have slightly decreased the experimental natural frequencies from that of a perfect theoretical beam. This suggested that although the Hill and Lin modulus of elasticity provided the closest approximation to the actual tests, it is likely that their values are slightly lower than the actual material properties in the specimens. The specifications provided by Hill and Lin produced models whose results were less than 2% off of the actual natural frequencies which means that their method of determining the material properties was most likely better than that of both of the manufacturer and the results found in the static experiments performed in this thesis. The experimental method of determining the modulus of elasticity may have been slightly flawed even though it was verified using a material with known material properties. This error could have come from the fact that the digital indicator used was not able to measure in small enough increments to give the actual deflection of the beam. The aluminum beam test had a much lower modulus of elasticity which means that the beam's deflection was much greater than that of the 85% TiB-15% Ti specimens. The lack of a high enough resolution could have affected the results. Also, it was possible that the experimental values found for the density and modulus of elasticity were accurate and the 6.73% difference from the experimental results could have been due to the imperfect clamp and the mass of the accelerometer on the beam. Another experiment using a vibrometer to measure the natural frequencies non-intrusively could be useful in determining the effects of the accelerometer on the beam. The vibrometer does not physically touch the specimen, but uses a laser to measure the vibrations. This allows the

measurement of the natural frequencies without adding mass to the end of the specimen which has a slight impact on its natural frequency.

When comparing the three methods described above in the Finite Element Development section, the plane strain analysis was found to be the closest approximation to the experimental results. The comparison for the three models can be seen in Table 14 below.

**Table 14. Model Comparison**

<b>Mode</b>	<b>Experimental Frequency (Hz)</b>	<b>Plane Stress Frequency (Hz)</b>	<b>% Difference</b>	<b>Plane Strain Frequency (Hz)</b>	<b>% Difference</b>	<b>Plate Frequency (Hz)</b>	<b>% Difference</b>
<b>1</b>	388.80	381.70	1.83	387.35	0.37	383.56	1.35
<b>2</b>	2430.00	2382.20	1.97	2417.30	0.52	2394.80	1.45
<b>3</b>	6850.00	6626.40	3.26	6723.10	1.85	6677.20	2.52

These results were found using the modulus of elasticity provided by Hill and Lin and density by Chandran, Panda and Sahay, as they produced the most accurate model of the beam in the study above. Though the plane strain analysis was the closest approximation (0.37% difference), it was possible that this was merely a coincidence because the modulus of elasticity found by Hill and Lin may have been too low. The modulus of elasticity affected the values for the natural frequency considerably. When higher values of modulus of elasticity were used in the model the plane strain analysis quickly failed to be the best approximation as it produced the highest values of the three models studied. Plane strain requires the width of the beam to be 10 times greater than the length of the beam to achieve a true plane strain condition and plane stress requires that the width needs to be infinitesimally small. The width of the specimen was in between these two extremes as should be the values for natural frequency if one were

able to model the specimen exactly. Therefore it was reasonable to accept the frequency results from the plate which took into account the actual width of the beam instead of merely assuming it to be infinite or infinitesimal as the plane strain and plane stress analyses did. Also, the size of the mesh required (800 nodes in the length direct for the plane strain/stress analysis compared with 50 nodes in the plate analysis) and consequently the amount of computing time necessary was reduced greatly when using the plate model. The greatest benefit for using the plane strain/stress element over the plate was the fact that the plane strain/stress element allows one to see what is happening inside the beam in terms of stress concentrations. If only the modes and not the stress concentrations within the beam were required, the plate analysis would be a better model.

The mode shapes for the homogeneous beam can be seen in Figure 40, Figure 41 and Figure 42 below. This was what one would expect to see for the first three bending modes for a homogeneous material cantilevered at one end.

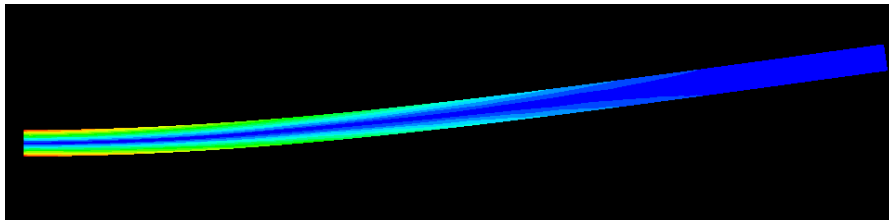


**Figure 40. Homogeneous Mode 1**

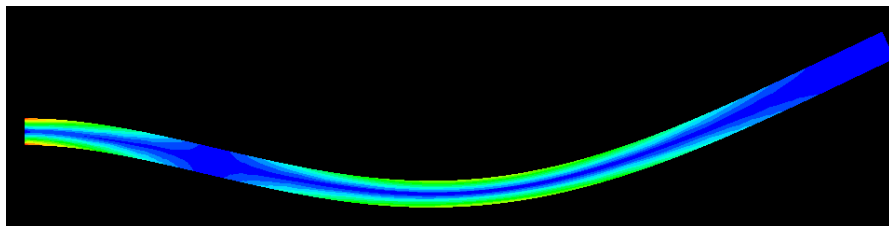


**Figure 41. Homogeneous Mode 2**

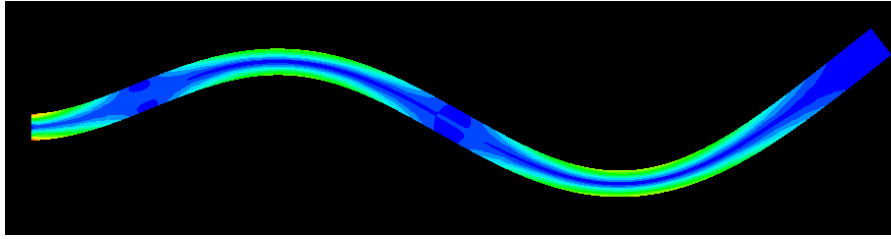


**Figure 42. Homogeneous Mode 3**

In these figures the relative stress concentrations can be seen with blue being zero stress and red being the highest stress concentrations. It should be noted that the stresses are nearly symmetric from one side of the beam to the other with the center of the beam remaining at zero stress. This was what one would expect to see for a homogenous beam. These mode shapes were compared to the mode shapes for the FGM in Figure 43, Figure 44 and Figure 45 below.

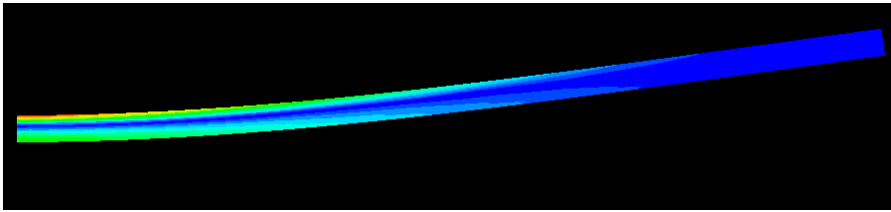


**Figure 43. FGM Mode 1**

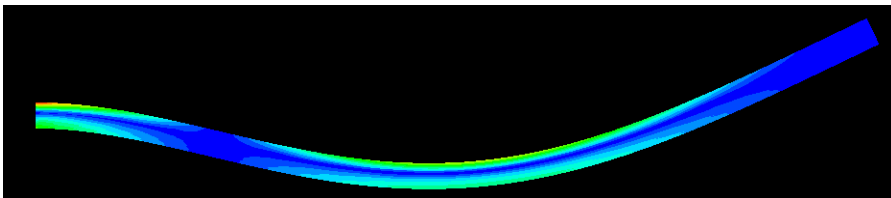


**Figure 44. FGM Mode 2**

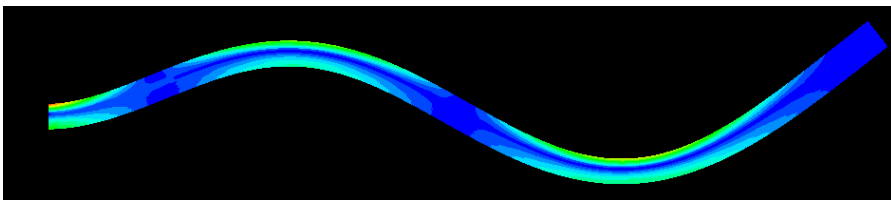


**Figure 45. FGM Mode 3**

It was seen that the mode shapes were nearly identical as those of the homogenous beam. This makes physical sense because the material properties were only changing in the thickness direction and not the length direction. If the material properties were to change along the length, a different shape would be expected for the bending modes. Also the relative stress concentration should be noted as compared with Figure 40, Figure 41 and Figure 42 above. The stress concentrations were higher on the upper surface of the beam than they were on the lower surface. This was due to a higher modulus of elasticity on the upper portion of the beam with the same deflections as the lower portion. This created larger stress concentrations.

The results for the FGM models can be seen in Table 15 below. This data was found using the average dimensions and experimental frequencies as seen in Table 8 above. The percent difference for each model is shown below the theoretical results for each model.

**Table 15. FGM Model Comparison**

<b>Model</b>	<b>Mode 1 (Hz)</b>	<b>Mode 2 (Hz)</b>	<b>Mode 3 (Hz)</b>
<b>Plane Stress</b>	304.3	1899.3	5284.3
<i>% Difference</i>	<i>6.1</i>	<i>4.1</i>	<i>3.1</i>
<b>Plane Strain</b>	314.9	1964.9	5465.5
<i>% Difference</i>	<i>9.7</i>	<i>7.7</i>	<i>6.6</i>
<b>Plate</b>	307.4	1918.7	5353.5
<i>% Difference</i>	<i>7.1</i>	<i>5.2</i>	<i>4.4</i>

It can be seen that the most accurate model for the FGM was the plane stress unlike the homogeneous tests above. This was due to the fact that the plane stress analysis provided the lowest estimate for the natural frequencies and all the values were above the experimental results. It was also mentioned above that modulus of elasticity values are likely slightly below the actual values in the Hill and Lin specifications which

were used in this study. This means that if these higher values would be used, the values for the natural frequencies would increase and create a larger percentage difference between the models and the experiment. This implies that there may be an interaction between the layers or a byproduct of the manufacturing process which affects the modeling of the FGM. A difference of 7.1% for the first mode in the plate model is not ideal, but it provides an estimate for the beam. This difference could be due to many factors such as inaccurate material properties for the inner layers of the beam, the densities not being exact, or variation in the thickness of the specimens. Also, the clamping method might not be ideal producing slightly lower experimental frequency results than theory would suggest. Though, because the same clamping method was used which produced results to 1.35% difference for the homogeneous beam using the Hill and Lin specifications, error from the clamping method can be assumed to not drastically affect the experimental results. Another possibility for error was the fact that the dimensions of the inner layers of the beam were possibly not the same as what the manufacturer reported. A study was completed to determine the effects of manipulating the inner layer thicknesses of the beam. The uppermost layer of the beam (85% TiB-15% Ti) was allowed to shrink as the sixth layer from the top (15% TiB-85% Ti) was increased in thickness. The results from this test can be seen in Table 16 below.

**Table 16. FGM Layer Thickness Variation**

<b>Layer 1 Thickness (cm)</b>	<b>Layer 6 Thickness (cm)</b>	<b>Mode 1 (Hz)</b>	<b>Mode 2 (Hz)</b>	<b>Mode 3 (Hz)</b>
<b>0.0886</b>	<b>0.04064</b>	304.28	1899.3	5284.3
<i>% Difference</i>		6.1	4.1	3.1
<b>0.0876</b>	<b>0.04164</b>	304.07	1897.9	5280.4
<i>% Difference</i>		6.0	4.0	3.0
<b>0.0866</b>	<b>0.04264</b>	303.89	1896.8	5277.1
<i>% Difference</i>		5.9	4.0	2.9
<b>0.0786</b>	<b>0.05064</b>	302.53	1888.1	5252.5
<i>% Difference</i>		5.4	3.5	2.4

The variation in layer thickness was suggested by the manufacturer. No specifics were given besides the fact that layer one may be slightly thinner than the specifications suggested and layer six might be slightly thicker. Also, this variation would cause the largest amount of change in the natural frequencies as layer one was the layer with the highest modulus of elasticity and layer six was the layer with the lowest modulus of elasticity besides the foil of pure titanium which was assumed to be a fixed thickness. As seen above, a variation in the thicknesses of the layers does not drastically impact the natural frequencies. When the thickness of the stiffest layer was decreased by 12.7% the difference was only decreased 0.7%. Though this does not drastically change the results for the natural frequencies, one can see the affect of making small adjustments in one of the many variables in the FGM. Small differences in material properties or geometries could easily make up for the 7.1% difference which was present in the plate model. Thus it was of the utmost importance to have accurate material properties for each of the individual layers as well as the correct dimensions for the thickness of each layer. This does not account for any discrepancies which might come from layer interaction within

the FGM or affects of the manufacturing process on the material properties which could also have an impact on the modeling of the material.

These results, although not perfect, provide an estimate of the actual characteristics of the FGM. Unlike the homogenous material, the plane stress model produced the results closest to those of the experiment. Like the homogenous models this could also be a coincidence because all of the models produced values which were above those of the experiment. These results will be helpful for future research into this material and these specimens in particular. It should merely be understood that the results produced by the Abaqus model were around 7% higher than the experimental results for this material. Further testing involving more accurate methods of determining material properties and a larger sample size of specimens should be used to create new specifications if more accurate results are desired.

The analysis of the stresses present in the specimen required the ultimate strength for the individual layers of the FGM. The ultimate tensile strength specification for TiB was measured by the manufacturer at various temperatures. Though, the values required interpolation in order to achieve values for the specific layer compositions. A value of 280 MPa was determined by the manufacturer to be the ultimate strength at 25°C for pure TiB [18]. The manufacturer also specified the ultimate strength for the commercially pure titanium to be 720 MPa at 25°C. These values may not be exact due to the fact that when the titanium was affixed to the FGM, it became more brittle, as was discussed in the fracture surface analysis above. Though, these values do provide an estimate for the material properties. These two values were combined using the rule of mixtures to produce ultimate strengths for each of the layers as seen in Table 17 below.

**Table 17. Ultimate Strength**

<b>Percent Ceramic Composition</b>	<b>Ultimate Strength (Mpa)</b>
85	346
75	390
60	456
45	522
30	588
15	654
0	720

The upper layer had the lowest ultimate strength (346 MPa) compared with the other layers and contained the highest stress concentrations as seen the in the visual Abaqus results in Figure 46 below.

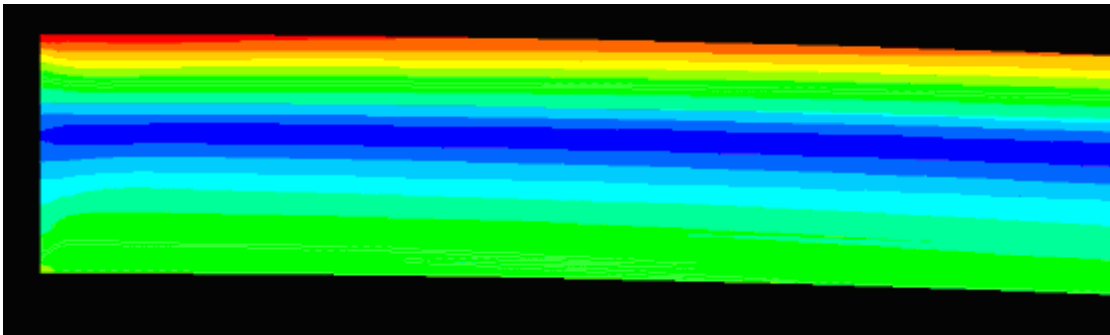


**Figure 46. FGM Maximum Stress Location**

Red was the highest stress and blue represented the lowest stress. A sinusoidal forcing function was applied to the free end of the beam. This forcing function was intended to simulate a cyclic load which could be applied using a shaker table for the study of the fatigue characteristics of the material. The forcing function can be seen in Figure 47 below.

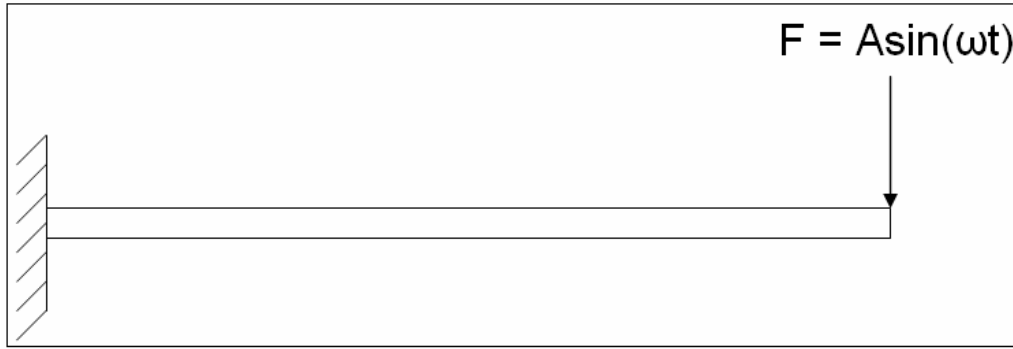


**Figure 47. Forcing Function**

The amplitude (A) of the forcing function was set to one Newton and produced a normal stress of 59.1 KPa in the top portion of the beam while only 38.9 KPa was present in the bottom layer. In order to reach the ultimate strength (failure) of the upper layer of the beam (346 MPa), it was necessary to increase the amplitude in the forcing function to 5.85 KN. In order to reach the ultimate strength of the bottom portion of the beam (720 MPa) it was necessary to increase the amplitude of the forcing function to 18.5 KN. It can be seen that well before the 18.5 KN force would be reached (required to fail the lower portion of the beam) the upper surface of the beam would reach failure. The values used in Table 17 for the ultimate strength only give an approximate value for the failure of the beam as the exact values for the ultimate strength of the FGM are not certain. In order to gain confidence in these values, a tensile test to failure should be performed on the homogeneous material of the beam. The force required to fail the beam will give a more accurate ultimate strength of the upper layer of the beam (which is the critical layer, dictating the failure of the specimen) and will allow for improved modeling in Abaqus. The same approach used for finding the maximum amplitude of the forcing function necessary to fail the beam, can also be used to find the stresses present in the beam at a lower amplitude for use in a fatigue test. The value for the amplitude can be explicitly

stated in the Abaqus program and the stresses displayed in the report will reflect the actual stresses present in the beam. Also, any desired stress level can be achieved by using a linear relationship between load and internal stresses to scale the forcing function amplitude of the sinusoidal load. For example, if one wanted to run a fatigue test that caused the stress in the upper layer of the beam to reach half of the ultimate strength, the amplitude would be set to half of that required to reach the ultimate strength (2.93 KN). These results should be used as approximations only, as experimental testing should be used to verify the Abaqus results.

## **Summary**

Two experiments were performed on the FGM specimens and included a static modulus of elasticity test as well as a dynamic natural frequency test. These tests were both conducted to help determine the actual material properties of the specimens as well as to help characterize the behavior of the material. Also, a study was completed to examine the effects of the clamp on the natural frequency results. The damping coefficient was also found using the logarithmic decrement method from the time history data produced in the dynamic vibrations test. The density was also found by finding the mass of the specimens and dividing by the volume of each of the specimens. This data was compared with densities found for the same material by Chandran, Panda and Sahay.

An optical microscope was used to examine the layers within the FGM. A specimen was polished and photographed under 50 and 200 times magnification to study the characteristics of the layering. Also a fracture surface was examined to determine the

failure modes present in the material and to determine the possible implications this presented for future research with this material.

Matlab was used to obtain a general understanding of the finite element method as well as to produce an estimate for the first natural frequency for the specimen. A study was completed to determine the affects of changing the number of elements in the model.

Finally Abaqus was used to model the specimen and was compared with the actual specimens to help determine the actual material properties present in the FGM. Different models, such as the plane strain/stress and plate element, were also experimented with to determine the effect the model had on the natural frequency results. The mode shapes for the FGM were also examined and compared with the mode shapes for a homogeneous material. Also, variations in the layer thicknesses within the specimen were studied to determine the effect on the natural frequency of the specimen. Finally, the stress concentrations present in the specimen were considered, and an approximate maximum amplitude for cyclic loading was found by comparing the finite element stress values with the ultimate strengths of the material.

## **IV. Conclusions and Recommendations**

### **Chapter Overview**

This chapter summarizes the findings of the experiments and the Abaqus models created in this thesis. Also, recommendations for action with this specific material are discussed along with recommendations pertaining to the modeling techniques. Finally, recommendations for future research are made to further the characterization of this material.

### **Conclusions**

This thesis included both experimentation and computational analysis to characterize functionally graded materials. The experimentation consisted of a static test and a dynamics test. Results from these tests were studied and compared with the findings from models generated with a commercial finite element analysis software package (Abaqus). A Matlab finite element code was also developed to create a baseline for comparison with the Abaqus to gain confidence in the Abaqus models. This code also allowed the insight into the mathematics involved in the finite element method.

The static experiment was conducted to generate a modulus of elasticity for each of the specimens. It was found that the experimental results for the modulus of elasticity were about 17% higher than the experiments conducted by Hill and Linn and about 11% lower than the modulus of elasticity claimed by the manufacturer. This large discrepancy between three different sources (the manufacturer's specifications, Hill and Lin's study

and the experimental results) was a testament to the difficulty in finding accurate values for the material properties of an FGM. Though these material properties varied considerably it was found in the dynamic testing that the actual modulus of elasticity was most likely slightly higher than that found by Hill and Lin and slightly lower than the experimental results. Dynamic testing was required to help determine the material properties for use in the stress analysis models

The dynamic testing provided insight into various material properties of the FGM. The first three natural frequencies for each of the specimens were found using the dynamic vibrations test and were used to verify the material properties. These values for the natural frequency were then compared to a similar vibrations test using a different clamping method. This test was performed to determine the affect of the clamp on the results for the natural frequencies. It was determined that vertical post clamp used as a comparison lowered the first natural frequency nearly 2% for specimens four and seven and approximately 0.5% for specimen one in sheet 974-1. This showed that the clamping method did have a slight impact on the results of the test and should be taken into account for the analysis of error. The dynamic tests also provided a time history of the vibrations in the beam which were used to find the damping coefficients. It was found that the FGM had a slightly higher damping coefficient of 0.00155 compared with the homogenous material (85% TiB-15% Ti) which had a coefficient of 0.00105.

The average densities for the specimens were also measured and compared with the values found by Chandran, Panda and Sahay. It was found that the densities found in the experiment were less than 3% different than those found in Chandran's study. The

different densities were compared in the Abaqus models to determine the effects of the densities on the natural frequencies.

The polished surface for one of the specimens was examined under a microscope to determine if any conclusions could be made about the layer thickness. It was found that the upper layer of the FGM was most likely thinner than the manufacturer suggested while layer five or six may have been slightly thicker. This finding led to an Abaqus study which was conducted to examine what affect changing the dimensions of the inner layers had on the natural frequencies. It was found that decreasing the thickness of the upper layer by 12.7% only decreased the difference in the natural frequency by 0.7%, but it was shown that this could have an affect on the material properties when combined with other sources of uncertainty within the FGM.

A scanning electron microscope was used to examine a fracture surface of one of the FGM specimens to examine the failure characteristics of the FGM. It was found that the entire cross section failed in a brittle manner which was unexpected. This suggested that the titanium, which is normally a relatively ductile material, was made more brittle through the manufacturing process. This could be due to boron particles seeping into the pure titanium foil during the high temperature manufacturing of the material. It is important to understand that this embrittlement of the titanium creates a disadvantage for the material as it loses some of its fracture toughness.

Abaqus models were created to approximate the actual behavior of the material and to help predict future behavior of more complex structures. The homogeneous material consisting of 85% TiB and 15% Ti was modeled first and it was determined that the closest modulus of elasticity values available were those published by Hill and Lin.

This was found by comparing the modeled natural frequencies with the experimental natural frequencies and doing a study as to which modulus of elasticity gives the closest results to the experiments. Also different modeling techniques were examined and it was found that the plate produced the most accurate results for the natural frequencies, but the plane stress/strain models provided insight into the stresses present in the thickness direction of the specimen. The mode shapes were also compared for the homogenous material and the FGM in Abaqus. It was determined that the functional grade had no impact on the shape of the mode because the function varied the material properties in the thickness direction rather than the length direction.

Finally a study was conducted to find the amplitude necessary to fail the specimen under cyclic loading. A sinusoidal load was applied to the end of the beam and the amplitude was scaled to the point where the maximum stresses present in the beam reached that of the ultimate strength of the material. The amplitude of the force required to reach failure in the upper layer of the beam was 5.85 KN. This value can be scaled down to achieve any stress level below the ultimate strength of the specimen. This will be important for future testing of the beam including cyclic loading tests to examine the fatigue properties of the material.

### **Recommendations for Action**

One important lesson that was learned was not to blindly trust the manufacturer's specifications. It was shown that the values they published for the material properties were not actually the same as those present in the specimens they produced. If possible, further testing should be conducted to find the actual material properties. Also, for this

specific FGM it should be understood that the values produced for the FGM in the Abaqus model were around 7% higher than the experimental results. This provides a reasonable estimate for what the natural frequency values for each specimen will be when they undergo further testing in the future, to include cyclic loading at the first natural frequency.

### **Recommendations for Future Research**

FGMs are a relatively new material and the potential for future research is promising in this area of materials science. The specific FGM used in this experiment lends itself to further study in other areas to help characterize this material and to determine the effectiveness of the material in future applications.

Because of the difficulty in finding the actual material properties for the layers of the FGM without using destructive testing, a study could be conducted to find these values using destructive methods. Methods of testing the modulus of elasticity, the density, the ultimate strengths and the other thermal coefficients are available and could be used to gain a further understanding of how the manufacturing process affects the material properties and the impact that has on the performance of this material. Larger sample sizes of specimens would be a benefit to obtain a more statistically sound value for these material properties.

Also, the information obtained in the study of this thesis can be used to further study the behavior of the material under cyclic loading. It is possible to determine the fatigue properties of the material and to develop an *S-N* curve which characterizes the material. This information could be used to study the effects of changing the internal

function of the FGM. It may be possible to generate an  $S-N$  curve and use it to predict the behavior in other FGMs with different internal functional variations with similar outer layers. If this is possible, the fatigue properties could be generated for an entire class of FGMs with a single  $S-N$  curve.

Variations in temperature gradients applied to this material should also be studied. FGMs are only beneficial in harsh temperature gradient environments, so it would be valuable to study how effective they are at providing thermal protection. This should be modeled in Abaqus as well as compared with experimentation. Elevated temperature gradients could also be studied in the cyclic loading tests to determine the effects of temperature on the fatigue properties of the material.

## **Summary**

The experiments and models generated in this research were able to characterize some of the important material properties and material behaviors for the FGM. Analytical results were compared with experimentation to add validity to the modeling techniques used in most FGM research today. It was found that the finite element method was only as good as the material properties present in the models. It was found that the hardest part of creating an accurate model was not the generation of the models, but the determination of the true material properties and the effects the manufacturing process may have had on the material.

The future is bright for this engineered material as it may be possible to achieve the beneficial thermal characteristics of ceramics along with the desired strength characteristics of metal without a single point of contact causing a large stress

concentration and premature failure. As the research into this material continues and the process for manufacturing this material improves, the applications in many industries will become apparent. It is clear that there are benefits to using functionally graded materials, though it remains to be tested and proven as a beneficial and plausible solution to the high load, harsh thermal gradient applications within industry.

## Appendix A: Matlab Code

```
clear;clc;

% Find natural frequency of beam
% 2Lt Ben Chapman

% Beam geometry and material properties

b = .024505; % meters
h = .003150; % meters
L = 0.1016; % meters
rho = 4373.8; % kg/m^3
m = rho*(b*h*L); % Kg using 85% TiB 15% Ti material properties
E = 274.3*10^9; % Pa using same
Iz = 1/12*(b)*(h)^3; % m^4

% Select number of elements for beam mesh
elements=30;
nodes=2; % Every beam element has two nodes

% Connectivity matrix which will be used to assemble k matrices for
% multiple elements within the beam is initialized
connect = zeros(elements,nodes);

% Create a connectivity matrix for any number of elements
for i=1:elements;
    for j=1:nodes;
        connect(i,j)=connect(i,j)+i+1*(j-1);
    end
end
connect

% Determine the size of the global k matrix
N = max(connect(:))*nodes;

% Adjusts length for any number of elements inputed above
L1=L/elements;

% Solve for mass of each individual element
mass1 = m/elements;

% Initialize a global k matrix for inputs for any number of elements (from
% above)
K = zeros (N,N);
```

```

M = zeros (N,N);
for e = 1:elements

    k = (E*Iz)/L1^3*[12 6*L1 -12 6*L1;6*L1 4*L1^2 -6*L1 2*L1^2;-12 -6*L1 12 -
6*L1;...
    6*L1 2*L1^2 -6*L1 4*L1^2];

    mass = (mass1/420)*[156 22*L1 54 -13*L1;22*L1 4*L1^2 13*L1 -3*L1^2;...
    54 13*L1 156 -22*L1;-13*L1 -3*L1^2 -22*L1 4*L1^2];

    for n = 1:nodes;
        for p = 1:nodes;
            K(connect(e,n)*2-1,connect(e,p)*2-1) = K(connect(e,n)*2-1,connect(e,p)*2-
1)+k(n*2-1,p*2-1);
            K(connect(e,n)*2-1,connect(e,p)*2) = K(connect(e,n)*2-1,connect(e,p)*2)+k(n*2-
1,p*2);
            K(connect(e,n)*2,connect(e,p)*2-1) = K(connect(e,n)*2,connect(e,p)*2-
1)+k(n*2,p*2-1);
            K(connect(e,n)*2,connect(e,p)*2) = K(connect(e,n)*2,connect(e,p)*2)+k(n*2,p*2);

            M(connect(e,n)*2-1,connect(e,p)*2-1) = M(connect(e,n)*2-1,connect(e,p)*2-
1)+mass(n*2-1,p*2-1);
            M(connect(e,n)*2-1,connect(e,p)*2) = M(connect(e,n)*2-
1,connect(e,p)*2)+mass(n*2-1,p*2);
            M(connect(e,n)*2,connect(e,p)*2-1) = M(connect(e,n)*2,connect(e,p)*2-
1)+mass(n*2,p*2-1);
            M(connect(e,n)*2,connect(e,p)*2) =
M(connect(e,n)*2,connect(e,p)*2)+mass(n*2,p*2);

        end
    end
end
K
M % This is the mass matrix for a beam element

for z = 3:N
    for w = 3:N
        K1(z-2,w-2) = K(z,w);
        M1(z-2,w-2) = M(z,w);
    end
end
% This step uses the Choleski Method as seen on pg 670 of Cook's FEA text
U = chol(M1)

```

```

% This step creates a matrix which can be solved for Eigenvalues and
% vectors...this is the Au matrix as seen at the bottom of pg 677 in Cook's
% text.
system = inv(U)*K1*inv(U)

% Solve for eigenvalues and eigenvectors
[mode,eigenvalues]=eig(system)

% Find the natural frequency from the eigenvalues
naturalfrequency = sqrt(eigenvalues)/(2*pi);
fprintf('Natural Freq: %.3f\n',naturalfrequency);
mode;

```

## Appendix B: Sample Abaqus Report

Field Output reported at nodes for Region(s) FGM-1: solid < TIB-75 >

Computation algorithm: EXTRAPOLATE\_COMPUTE\_AVERAGE

Averaged at nodes

Averaging regions: ODB\_REGIONS

Node Label	UT.U2 @Loc 1	S.Max. Prin @Loc 1	S.S11 @Loc 1	S.S12 @Loc 1
1	-576.779E-09	745.752	743.78	-68.8317
2	704.958E-42	20.179E+03	19.9973E+03	1.77294E+03
15	-576.815E-09	2.63766E+03	2.20291E+03	-2.28963E+03
16	18.5876E-39	59.3819E+03	59.1224E+03	-3.79253E+03
17	-575.718E-09	372.876	111.605	-299.099
18	-574.651E-09	88.8977	-225.657	-435.607
19	-573.59E-09	203.052	-53.37	-487.966
20	-572.523E-09	201.211	-266.617	-571.337
21	-571.462E-09	230.358	-177.352	-444.545
22	-570.395E-09	294.823	-174.339	-452.847
23	-569.334E-09	292.468	-122.501	-355.006
24	-568.267E-09	311.72	-32.694	-332.847
25	-567.206E-09	331.846	8.72786	-299.724
26	-566.139E-09	352.1	98.1153	-277.969
27	-565.078E-09	378.471	133.51	-277.801
28	-564.012E-09	405.984	205.549	-262.1
29	-562.951E-09	435.289	236.956	-274.512
30	-561.884E-09	465.288	293.518	-264.079
31	-560.823E-09	495.664	322.445	-279.653
32	-559.757E-09	524.991	368.079	-272.823
33	-558.696E-09	554.545	395.563	-287.705
34	-557.631E-09	582.237	433.971	-283.133
35	-556.569E-09	610.385	460.654	-295.986
36	-555.504E-09	636.468	494.363	-292.774
37	-554.443E-09	663.285	520.617	-303.335
38	-553.378E-09	688.081	551.277	-300.927
39	-552.316E-09	713.84	577.304	-309.362
40	-551.252E-09	737.708	605.981	-307.434
41	-550.19E-09	762.695	631.883	-314.056
42	-549.126E-09	785.947	659.272	-312.423
43	-548.065E-09	810.403	685.101	-317.562
44	-547.001E-09	833.29	711.66	-316.131
45	-545.939E-09	857.402	737.439	-320.092
46	-544.876E-09	880.113	763.471	-318.815
47	-543.814E-09	904.018	789.21	-321.854

## Appendix C: Displayed Node Numbers

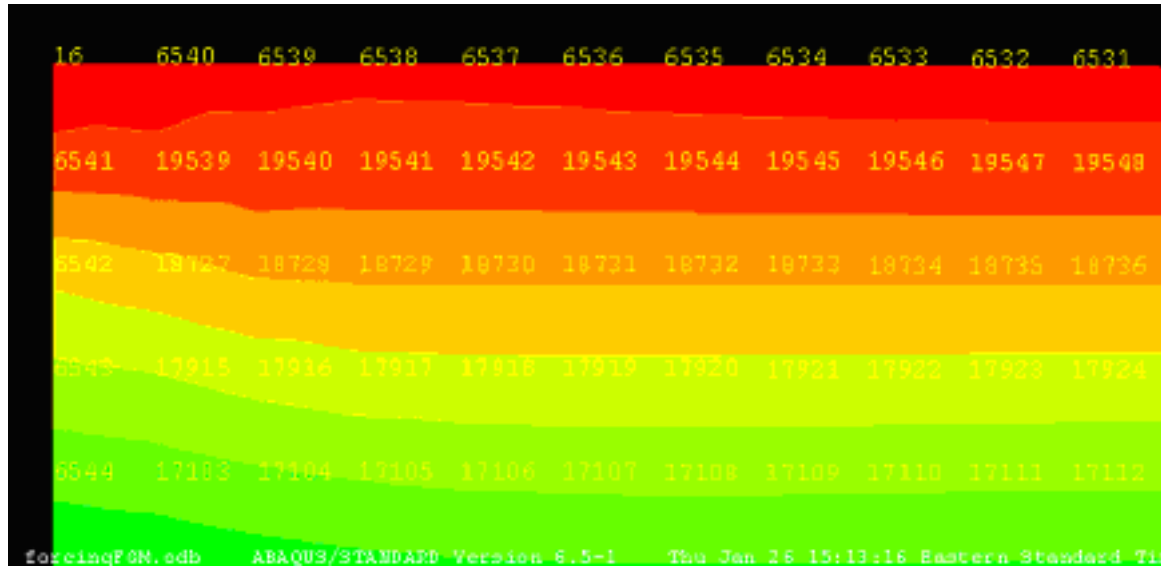


Figure 48. Node Numbers

## Bibliography

1. Aboudi, J., Pindera, M.J., Arnold, Steven M. "Higher Order Theory of Functionally Graded Materials," <http://www.grc.nasa.gov/WWW/RT2000/5000/5920arnold3.html>, 2001.
2. Chandran, Ravi K.S., Panda, K.B., Sahay, S.S. "TiB<sub>w</sub>-Reinforced Ti Composites: Processing, Properties, Application Prospects, and Research Needs," <http://www.tms.org/pubs/journals/JOM/0405/Chandran-0405.html>, Salt Lake City UT, 2004.
3. Cobb, Richard. Class Notes, Structural Dynamics. School of Engineering and Management, Air Force Institute of Technology, Wright-Patterson AFB OH, 2006.
4. Cooley, William G. "Application of Functionally Graded Materials in Aircraft Structures." Wright Patterson AFB OH: AFIT Thesis, 2005.
5. Cooley, William G., Palazotto, Anthony N. "Finite Element Analysis of Functionally Graded Shell Panels Under Thermal Loading." Orlando FL: IMECE Conference, IMECE2005-82776, 2005.
6. Cook, Robert D., Malkus, David S., Plesha, Michael E., Witt, Robert J. *Concepts and Applications of Finite Element Analysis* (4<sup>th</sup> Edition). New York NY: John Wiley & Sons, Inc., 2002.
7. Eason, Tomas G., Caraballo, Simon A. "A Comparison of Finite Element Beam Formulations for Thermoelastic Behavior of Functionally Graded Structures." Orlando FL: 2005 ASME International Mechanical Engineering Congress and Exposition, IMECE2005-80999, 2005.
8. Engineers Edge. "Structural Beam Bending Equations/Calculation Cantilevered Beam with Load at Location between Support and Load." [http://www.engineersedge.com/beam\\_bending/beam\\_bending10.htm](http://www.engineersedge.com/beam_bending/beam_bending10.htm), 2006.
9. Hibbeler, R. C. *Mechanics of Materials* (4<sup>th</sup> Edition). Upper Saddle River NJ: Prentice Hall International, Inc., 2000.
10. Hill, M.R., Carpenter, R.D., Paulino, G.H., Munir, Z.A., Gibeling, J.C. "Fracture Testing of a Layered Functionally Graded Material," *Fracture Resistance Testing of Monolithic and Composite Brittle Materials*, ASTM STP 1409, J.A. Salem, G.D. Quinn, and M.G. Jenkins, Eds., American Society for Testing and Materials, West Conshohocken PA, 2002.

11. Hill, Michael R., Lin, Wei-Yan. "Residual Stress Measurement in a Ceramic-Metallic Graded Material," *Journal of Engineering Materials and Technologies*, April 2002, Vol. 124, Davis CA: ASME, 2002.
12. Lee, Woo Y., Stinton, David P., Berndt, Christopher C., Erdogan, Frazil, Lee, Yi-Der, Mutasim, Zaher. "Concept of Functionally Graded Materials for Advanced Thermal Barrier Coating Applications." Oak Ridge TN: Contract No. DE-AC05-96OR22464 with Lockheed Martin Energy Research Corporation, 1996.
13. Logan, Daryl L. *A First Course in the Finite Element Method* (3<sup>rd</sup> Edition). Pacific Grove CA: Brooks/Cole, 2002.
14. MatWeb. <http://www.matweb.com/search/GetProperty.asp>, Automation Creation Inc., 2006.
15. Mendenhall, William. *Introduction to Probability and Statistics* (3<sup>rd</sup> Edition). Belmont CA: Wadsworth Publishing Company, Inc., 1971.
16. Na, Kyung-Su, Kim, Ji-Hwan. "Three-Dimensional Thermomechanical Buckling of Functionally Graded Materials," *AIAA Journal*, Vol. 43, No. 7, July 2005. Danvers MA: American Institute of Aeronautics and Astronautics, Inc., 2005.
17. Nelson, Greg. "RE: Order Delivery." Electronic Mail from [gregn@cercomceramics.com](mailto:gregn@cercomceramics.com) to Byrd, Larry W, AFRL/VASM. November 2005.
18. Palicka, Rich. "FW: WPAFB – Ti/TiB Property Data May 3, 05." Electronic Mail from [richp@cercomceramics.com](mailto:richp@cercomceramics.com) to Byrd, Larry W, AFRL/VASM. May 2005.
19. Panda, K.B., Chandran, Ravi K.S. "Synthesis of Ductile Titanium-Titanium-Boride (Ti-TiB) Composites with Beta-Titanium Matrix: The Nature of TiB Formation and Composite Properties," *Metallurgical and Materials Transactions A*, Volume 24A, Salt Lake City UT, 2003.
20. Reddy, J.N. "Analysis of Functionally Graded Plates," *International Journal for Numerical Methods in Engineering*, 47:663-384, College Station TX: John Wiley & Sons, Ltd., 2000.
21. Reddy, J.N. *Mechanics of Laminated Composite Plates and Shells* (2<sup>nd</sup> Edition). Boca Raton FL: CRC Press, LLC, 2004.
22. Simon, Steve. "Stats-Steve's Attempt to Teach Statistics." <http://www.childrens-mercy.org/stats/ask/rsquared.asp>, Children's Mercy Hospitals and Clinics, 2005.

23. Suresh, S., Mortensen, A. *Fundamentals of Functionally Graded Materials*. London UK: IOM Communications Ltd, 1998.
24. Wulpi, Donald J. *Understanding How Components Fail* (2<sup>nd</sup> Edition). Materials Park OH: ASM International, 2000.

## **Vita**

2<sup>nd</sup> Lt Benjamin Chapman graduated from Rockford High School in Rockford, Michigan in 2000. He then entered the United States Air Force Academy for his undergraduate studies earning a Bachelors of Science in Mechanical Engineering. He was commissioned as an officer on 2 June 2004 and was selected to attend graduate school as a direct accession from the Air Force Academy.

2<sup>nd</sup> Lt Chapman entered graduate school in the fall of 2004 studying at the Air Force Institute of Technology. While attending AFIT he studied Aeronautical Engineering with a focus in Structural Mechanics and Systems Engineering. Upon graduation, he will be assigned to the Air Force Research Laboratory in the Air Vehicles Directorate at Wright Patterson Air Force Base, OH.

REPORT DOCUMENTATION PAGE				Form Approved OMB No. 074-0188	
<p>The public reporting burden for this collection of information is estimated to average 1 hour per response, including the time for reviewing instructions, searching existing data sources, gathering and maintaining the data needed, and completing and reviewing the collection of information. Send comments regarding this burden estimate or any other aspect of the collection of information, including suggestions for reducing this burden to Department of Defense, Washington Headquarters Services, Directorate for Information Operations and Reports (0704-0188), 1215 Jefferson Davis Highway, Suite 1204, Arlington, VA 22202-4302. Respondents should be aware that notwithstanding any other provision of law, no person shall be subject to a penalty for failing to comply with a collection of information if it does not display a currently valid OMB control number.</p> <p><b>PLEASE DO NOT RETURN YOUR FORM TO THE ABOVE ADDRESS.</b></p>					
1. REPORT DATE (DD-MM-YYYY) 23-03-2006		2. REPORT TYPE Master's Thesis		3. DATES COVERED (From – To) Sep 04 – Mar 06	
4. TITLE AND SUBTITLE  Characterization of Functionally Graded Materials				5a. CONTRACT NUMBER	
				5b. GRANT NUMBER	
				5c. PROGRAM ELEMENT NUMBER	
6. AUTHOR(S)  Chapman, Benjamin, D., Second Lieutenant, USAF				5d. PROJECT NUMBER	
				5e. TASK NUMBER	
				5f. WORK UNIT NUMBER	
7. PERFORMING ORGANIZATION NAMES(S) AND ADDRESS(S) Air Force Institute of Technology Graduate School of Engineering and Management (AFIT/EN) 2950 Hobson Way WPAFB OH 45433-7765				8. PERFORMING ORGANIZATION REPORT NUMBER  AFIT/GAE/ENY/06-M05	
9. SPONSORING/MONITORING AGENCY NAME(S) AND ADDRESS(ES) AFRL/VASM Attn: Dr. Ravinder Chona 2790 D Street, Bldg 65 WPAFB OH 45433-7765 DSN: 674-6787				10. SPONSOR/MONITOR'S ACRONYM(S)	
				11. SPONSOR/MONITOR'S REPORT NUMBER(S)	
12. DISTRIBUTION/AVAILABILITY STATEMENT APPROVED FOR PUBLIC RELEASE; DISTRIBUTION UNLIMITED.					
13. SUPPLEMENTARY NOTES					
14. ABSTRACT <p>The purpose of this study was to characterize the behavior of a functionally graded material through experimentation and analytical modeling. Functionally graded materials are a ceramic metal composite which transitions from metal on one face to ceramic on the opposite face. Creating reliable models required verifying the material properties. This was accomplished through the use of a static modulus of elasticity test as well as a dynamic ping test. The natural frequencies from the dynamic test were compared with finite element models to determine which material properties most accurately represented the functionally graded material. It was found that the material properties established experimentally by Hill and Lin produced the best models. A fracture surface was examined to determine the failure criteria for the prediction of failure in a cyclic loading scenario. It was determined that the material would fail in a brittle manner and the maximum principle stresses should be used to predict failure. Finally, a model was generated to analyze the through-the-thickness stresses in the material under a sinusoidal forcing function. It was determined that the majority ceramic upper layer was the critical layer for failure and required an amplitude of 5.83 KN to reach failure in the specimen.</p>					
15. SUBJECT TERMS Functionally Graded Materials, Finite Element Analysis, Ceramic Metal Composite, Material Properties, Analytical Modeling, Experimental Testing, Stress Analysis, Failure, Cyclic Loading					
16. SECURITY CLASSIFICATION OF:			17. LIMITATION OF ABSTRACT  UU	18. NUMBER OF PAGES  114	19a. NAME OF RESPONSIBLE PERSON Dr. Anthony N. Palazotto
REPORT U	ABSTRACT U	c. THIS PAGE U			19b. TELEPHONE NUMBER (Include area code) (937) 255-3636, ext 4599; e-mail: anthony.palazotto @afit.edu